

Model-based Super-resolution: Towards a Unified Framework for Super-resolution

Zetao Fei ^{*} and Hai Zhang [†]

July 25, 2024

Abstract

In mathematics, a super-resolution problem can be formulated as acquiring high-frequency data from low-frequency measurements. This extrapolation problem in the frequency domain is well-known to be unstable. We propose the model-based super-resolution framework (Model-SR) to address this ill-posedness. Within this framework, we can recover the signal by solving a nonlinear least square problem and achieve the super-resolution. Theoretically, the resolution-enhancing map is proved to have Lipschitz continuity under mild conditions, leading to a stable solution to the super-resolution problem. We apply the general theory to three concrete models and give the stability estimates for each model. Numerical experiments are conducted to show the super-resolution behavior of the proposed framework. The model-based mathematical framework can be extended to problems with similar structures.

1 Introduction

Appearing in different literature, super-resolution mainly refers to the techniques that enhance the resolution of signals or images. Since the birth of the microscope, super-resolution has been a central problem for imaging systems for about three centuries. In wave-based imaging systems, the resolution is limited due to the diffraction nature of the wave. The resolution limit can be characterized by Rayleigh length and depends on the cutoff frequency of the system. Super-resolution techniques are therefore widely desired in imaging-related fields such as geophysics [1], medical imaging [2], radar imaging [3], microscope [4], etc.

Enhancing the resolution requires a stable reconstruction of the high-frequency data from the low-resolution measurement. For a general compactly supported function, its Fourier transform is analytical, and hence the extrapolation problem enjoys uniqueness without noise. However, this problem is well-known to be ill-posed due to its instability in the presence of noise, as shown in the works [5, 6, 7]. For decades, the study of super-resolution

^{*}Department of Mathematics, HKUST, Clear Water Bay, Kowloon, Hong Kong (zfei@connect.ust.hk).

[†]Department of Mathematics, HKUST, Clear Water Bay, Kowloon, Hong Kong (haizhang@ust.hk). H. Zhang was partially supported by Hong Kong RGC grant GRF 16304621 and NSFC grant 12371425.

has primarily focused on the point source model. Originating from Prony’s method [8], various subspace methods have been developed for high-resolution point source reconstruction, including MUSIC [9], ESPRIT [10], and Matrix Pencil (MP) [11]. The analysis of these methods becomes complex when measurements are noisy. For discussions on the theoretical aspects of subspace methods, refer to [12, 13, 14] and the references therein. The significant advancements in compressive sensing over the past decades have motivated sparsity-exploiting algorithms for super-resolution, such as LASSO, TV norm minimization, atomic norm minimization, and B-LASSO [15, 16, 17, 18, 19, 20, 21, 22]. Theoretically, exact recovery and stability results are obtained under specific conditions, such as sources being separated by multiple Rayleigh lengths or other assumptions. In addition, the super-resolution problem for point sources has been investigated in [23, 24, 25, 26, 27] from an optimal reconstruction viewpoint, explaining the super-resolution capability of some algorithms. On the other hand, it is important to characterize the resolution limits for computational methods in the presence of noise. Recent studies [28, 29, 30] introduced the concept of computational resolution limit with quantitative characterization, and used it to explain the phase transition between successful reconstructions and unsuccessful ones with the presence of noise. See also further developments in [31, 32]. Despite the vast literature on super-resolution, few theoretical works have been done beyond the point source model. In a recent work [33], the authors assume the sources are combinations of point and dipole sources, taking a step forward.

The rapid development of computer vision brings wide literature on single-image super-resolution (SISR) methods for images. The example-based strategy [34, 35, 36, 37, 38, 39] was proposed before the boom of machine learning. In the latter approach, the idea that images with different resolutions form different low-dimensional manifolds with similar local geometry is explored and the representation scheme between these manifolds is studied. During the last decades, deep learning has developed and is applied to SISR. SRCNN [40] is proposed as the first convolutional neural network (CNN) based SISR method that learns the mapping from low-to-high-resolution images via hidden layers. Other models and architectures proposed for SISR include deep neural networks [41, 42], U-Net [43], adaptive models [44, 45, 46], generative adversarial networks (GAN) [47], and sparsity-based models [48, 49]. Due to the vast literature in this field, we refer interested readers to the surveys e.g. [50, 51].

1.1 Our Contribution

This paper develops the mathematical theory of model-based super-resolution framework (Model-SR). We explore the low-dimensional latent structure by adopting the idea that the signal space can be modeled by a low-dimensional parameter space. Similar ideas have been applied in various fields such as statistics [52], compressive sensing, image processing [53, 54], and machine learning [55]. Under the proposed framework, the numerical method for solving the super-resolution problem contains two steps. First, with the help of modeling, we can recover the signal by solving a nonlinear least square problem. Then, we get the resolution-enhanced signal by straightforward sampling. For a properly defined resolution-enhancing

map, see Section 2.1, we show that it is locally Lipschitz stable under mild conditions. We discuss several specific models under Model-SR. For the point source model, we derive the stability estimate which indicates that the exact recovery of point sources from the noiseless low-resolution measurement does not require a minimum separation distance condition. We extend our discussion to signals with a finite rate of innovation and signals that are continuous with a specific form, and we derive the corresponding stability results. Finally, numerical experiments are conducted to test the proposed method.

1.2 Organization of the paper

In Section 2, we introduce the model-based super-resolution framework. In Section 3, we consider the mathematical theory for the proposed framework with a focus on the stability estimate. We investigate the point source model within Model-SR in Section 4. We extend the discussion to signals with a finite rate of innovation and signals having a specific continuous form in the physics domain in Section 5 and Section 6 respectively. We conduct numerical experiments in Section 7. In Section 8, we discuss several extensions of the Model-SR. The paper concludes with a discussion of the proposed framework in Section 9.

1.3 Notations

Throughout the paper, we denote $\|\cdot\|$ the ℓ_2 norm and $\|\cdot\|_{op}$ the operator norm. We denote δ_θ for Dirac measure with support at $\{\theta\}$. For an operator \mathcal{A} , we denote $D\mathcal{A}$ the Fréchet derivative of \mathcal{A} . For a set U , $\mathcal{A}|_U$ represents the restriction of \mathcal{A} on U . We use the notation $C^k(U, V)$ for k -times continuously differentiable functions defined from U to V . For matrices $A, B \in \mathbb{C}^{n \times n}$, $A \preceq B$ means $B - A$ is positive semi-definite. We use $\sigma_{\min}(A)$ to denote the smallest singular value of A . We denote the identity matrix as \mathcal{I} and the identity map as id . The notation $B(a, r)$ represents the closed ball centered at a with radius r . We denote the Fourier transform of a function $f(x)$ as $\mathcal{F}f(\omega)$, defined by $\mathcal{F}f(\omega) = \int_{\mathbb{R}} f(x)e^{-2\pi i x \omega} dx$. Finally, we denote $[0, 1]_*$ the closed interval $[0, 1]$ equipped with the wrap-around distance $d_{\mathbb{T}}(a, b) = \min_{M \in \mathbb{Z}} |a - b - M|$.

2 Model-based Super-resolution Framework

In this section, we develop the model-based super-resolution framework (Model-SR). In Section 2.1, we introduce the main concepts and mathematical model. We discuss the numerical methodology in Section 2.2. Our presentation is restricted to one dimension for ease of presentation. The generalization to higher dimensions is straightforward.

2.1 Mathematical Model for Model-SR

In this section, we first present the general mathematical framework for super-resolution problems. Then, we propose the model-based super-resolution framework.

Let h be the sampling step size in the frequency domain, and $\omega_k = kh$, for $k \in \mathbb{Z}$. Denote the low-resolution sampling points as $\{\omega_k\}_{k=-K_L}^{K_L}$ and high-resolution sampling points as $\{\omega_k\}_{k=-K_H}^{K_H}$, where $K_H > K_L$. We define the super-resolution factor (SRF) as

$$\text{SRF} := \frac{K_H}{K_L}. \quad (2.1)$$

Let $\Omega \subset \mathcal{S}'(\mathbb{R})$, where $\mathcal{S}'(\mathbb{R})$ denotes the space of tempered distribution. For $\psi \in \Omega$, we define the low-resolution sampling operator $G_L : \Omega \rightarrow \mathbb{C}^{2K_L+1}$ as

$$G_L(\psi) = (g_{-K_L}(\psi), g_{-K_L+1}(\psi), \dots, g_{K_L}(\psi)), \quad (2.2)$$

with $g_k(\psi) = \mathcal{F}\psi(\omega_k)$. Similarly, we define the high-resolution sampling operator $G_H : \Omega \rightarrow \mathbb{C}^{2K_H+1}$ as

$$G_H(\psi) = (g_{-K_H}(\psi), g_{-K_H+1}(\psi), \dots, g_{K_H}(\psi)). \quad (2.3)$$

We assume that G_L and G_H are continuous. For $\psi, \tilde{\psi} \in \Omega$, We say ψ is sampling equivalent to $\tilde{\psi}$ if $g_k(\psi) = g_k(\tilde{\psi})$ for all $k \in \mathbb{Z}$. We define the signal space as an equivalent class, $[\Omega] := \Omega/\sim$. The motivation for such a definition can be seen in the example below.

Example 1. Let $\omega_k = k$, $\theta \in [0, 1]$, $\psi(x) = \delta_\theta$, and $\tilde{\psi}(x) = \delta_{1+\theta}$. Then, we can calculate that $g_k(\psi) = g_k(\tilde{\psi})$ for all $k \in \mathbb{Z}$ due to the fixed sampling step size. Thus ψ and $\tilde{\psi}$ are in the same equivalent class and they are viewed as the same signal.

For a slight abuse of notation, we use the notation Ω for signal space from now on.

Based on the definitions given above, we define the low- and high-resolution signal space as $\mathcal{H}_L := G_L(\Omega)$ and $\mathcal{H}_H := G_H(\Omega)$ respectively. Let $\mathcal{Q} : \mathcal{H}_H \rightarrow \mathcal{H}_L$ be the downsampling operator satisfying

$$\mathcal{Q} \circ G_H = G_L. \quad (2.4)$$

The diagram shown in Figure 1 commutes.

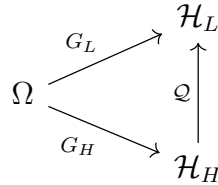


Figure 1: Signal space, low- and high-resolution spaces, and related maps.

Generally speaking, super-resolution aims to find a resolution-enhancing map, $\mathcal{L} : \mathcal{H}_L \rightarrow \mathcal{H}_H$, satisfying the following condition:

$$\mathcal{L} \circ G_L = G_H. \quad (2.5)$$

Combining (2.4) and (2.5), we have $(\mathcal{L}\mathcal{Q}) \circ G_H = G_H$, which implies that super-resolution essentially aims to find a generalized left inverse of the downsampling operator \mathcal{Q} .

To ensure the well-posedness of the super-resolution problem, we propose the following consistency condition:

Condition 1. *The low-resolution sampling operator G_L is injective.*

The above condition implies that we can determine the signal profile from the measurement. Otherwise, if there exist $\psi \neq \tilde{\psi} \in \Omega$ such that $G_L(\psi) = G_L(\tilde{\psi})$, then there exists some integer K_H such that $G_H(\psi) \neq G_H(\tilde{\psi})$. In this case, the resolution-enhancing map \mathcal{L} is not well-defined. In other words, the lack of Condition 1 results in the non-uniqueness of the super-resolution problem.

We remark that the signal space Ω should be properly chosen to make super-resolution possible. We use the following example for illustration.

Example 2. *Define*

$$\Omega_1 = \{\psi \in \mathcal{S}' : g_k(\psi) = 0, \forall |k| > K_L\}.$$

Then Condition 1 holds. For $\psi_1 \in \Omega_1$ and $K_H > K_L$, the resolution-enhancing map is given by

$$\mathcal{L}(G_L(\psi)) = (0, \dots, 0, g_{-K_L}(\psi), \dots, g_{K_L}(\psi), 0, \dots, 0). \quad (2.6)$$

In this case, super-resolution is impossible since no high-frequency information can be obtained from the low-frequency part.

Now, we are ready to introduce the model-based super-resolution framework.

Definition 1. *We say that Ω is modelable if there exists a compact parameter space $\Theta \subset \mathbb{R}^m$ and a map $\mathcal{P} : \Theta \rightarrow \Omega$, such that \mathcal{P} is surjective and continuous. We call \mathcal{P} the model map, (Θ, \mathcal{P}) a modeling pair. Further, we define the low-resolution map as $\mathcal{P}_L = G_L \circ \mathcal{P}$ and high-resolution map as $\mathcal{P}_H = G_H \circ \mathcal{P}$.*

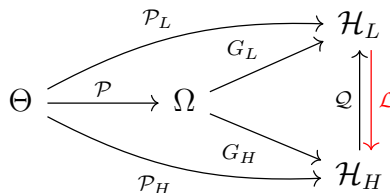


Figure 2: Model-based super-resolution framework.

Figure 2 illustrates the framework proposed above. By the surjection \mathcal{P} , the signal space can be regarded as a finite-dimensional manifold embedded in the infinite-dimensional space $\mathcal{S}'(\mathbb{R})$. To characterize the dimension of Ω , we introduce the following definition.

Definition 2. For modelable signal space Ω , we say that Ω has intrinsic dimension m if there exists a modeling pair (Θ, \mathcal{P}) with parameter space $\Theta \subset \mathbb{R}^m$ and $\dim \Theta = m$ satisfying that for any $\psi \in \Omega$, there exists a open neighborhood U_ψ and a discrete space Λ_ψ such that $\mathcal{P}^{-1}(U_\psi) = \bigsqcup_{d \in \Lambda_\psi} V_d$ and $\mathcal{P}|_{V_d}$ is a bijection for every $d \in \Lambda_\psi$.¹

Remark 2.1. By the continuity of \mathcal{P} and the compactness of Θ , it is easy to show $\mathcal{P}|_{V_d}$ is further a homeomorphism for every $d \in \Lambda_\psi$.

Notice that in the definition given above, we define the intrinsic dimension through the local bijection (homeomorphism) instead of the global one. This is because of the symmetry property of the model map \mathcal{P} , as in the following example.

Example 3. Let $\Theta = [0, 1]^2$, $\theta^{(1)} = (\theta_1^*, \theta_2^*)$, $\theta^{(2)} = (\theta_2^*, \theta_1^*)$, where $\theta_1^* \neq \theta_2^*$. Define $\mathcal{P}(\theta) = \delta_{\theta_1} + \delta_{\theta_2}$. Then, $\mathcal{P}(\theta^{(1)}) = \mathcal{P}(\theta^{(2)})$, though $\theta^{(1)} \neq \theta^{(2)}$.

In practice, the exact intrinsic dimension of the signal space may not be available and needs to be estimated. One may model Ω using more parameters. Thus, we introduce the following definition of compatibility for the case when the dimension of the parameter space is larger than the intrinsic dimension of signal space.

Definition 3. Let Ω be a modelable signal space with intrinsic dimension m and representation pair (Θ, \mathcal{P}) . Let $\tilde{\Theta} \subset \mathbb{R}^{\tilde{m}}$ with $\tilde{m} > m$, and $\tilde{\mathcal{P}} : \tilde{\Theta} \rightarrow \tilde{\Omega}$ be a continuous surjection such that $\Omega \subset \tilde{\Omega}$. Let $\tau_p : \Theta \rightarrow \tilde{\Theta}$ be the embedding, $\pi_p : \tilde{\Theta} \rightarrow \Theta$ be the projection such that $\pi_p \circ \tau_p = id_\Theta$. Let $\tau_s : \Omega \rightarrow \tilde{\Omega}$ be the embedding, $\pi_s : \tilde{\Omega} \rightarrow \Omega$ be the projection such that $\pi_s \circ \tau_s = id_\Omega$. We say (Θ, \mathcal{P}) and $(\tilde{\Theta}, \tilde{\mathcal{P}})$ are compatible if the diagram in Figure 3 commutes, i.e. $\mathcal{P} \circ \pi_p = \pi_s \circ \tilde{\mathcal{P}}$.

$$\begin{array}{ccc} \tilde{\Theta} & \xrightarrow{\tilde{\mathcal{P}}} & \tilde{\Omega} \\ \pi_p \downarrow & & \downarrow \pi_s \\ \Theta & \xrightarrow{\mathcal{P}} & \Omega \end{array}$$

Figure 3: Commute diagram for compatible modeling pairs.

We raise one simple example to illustrate the above definition.

Example 4. Let $\Theta = [0, 1]_*$, $\mathcal{P}(\theta) = \delta_\theta$, $\tilde{\Theta} = [0, 1]_*^2$, $\tilde{\mathcal{P}}(\theta_1, \theta_2) = \delta_{\theta_1} + \delta_{\theta_2}$. Let τ_p be defined by $\tau_p(\theta) = (\theta, 0)$, π_p be defined by $\pi_p(\theta_1, \theta_2) = \theta_1$, and $\tau_s = id_\Omega$. Let $U_\psi \subset \tilde{\Omega}$ be a neighborhood containing $\psi = \delta_{\theta_1} + \delta_{\theta_2}$, $V \subset \tilde{\Theta}$ be the open neighborhood containing (θ_1, θ_2) that satisfies $\tilde{\mathcal{P}}(V) = U_\psi$. We define $\pi_s = \mathcal{P} \circ \pi_p \circ \tilde{\mathcal{P}}|_V^{-1}$. It is easy to check π_s is well-defined and $\pi_s \circ \tau_s = id_\Omega$. Therefore, (Θ, \mathcal{P}) and $(\tilde{\Theta}, \tilde{\mathcal{P}})$ are compatible.

¹The symbol \bigsqcup denotes the disjoint union.

Consequently, we define the low-resolution map $\tilde{\mathcal{P}}_L$ from $\tilde{\Theta}$ to \mathcal{H}_L by $\tilde{\mathcal{P}}_L := G_L \circ \mathcal{P} \circ \pi_p = G_L \circ \pi_s \circ \tilde{\mathcal{P}}$. Similarly, we define the high-resolution map by $\tilde{\mathcal{P}}_H := G_H \circ \mathcal{P} \circ \pi_p = G_H \circ \pi_s \circ \tilde{\mathcal{P}}$.

We end this section with a remark on the low-resolution sampling operator G_L . Notice that for a given signal space, the choice of modeling pair (Θ, \mathcal{P}) is not unique and the model map \mathcal{P} may not be injective. Thus, it is meaningless to discuss the uniqueness in the parameter space. However, the injectivity of G_L ensures that starting from any modeling pair (Θ, \mathcal{P}) , we can always end up with the unique signal. It then offers the possibility to determine the signal from the low-resolution measurement numerically.

2.2 Numerical Methodology

In this section, we consider the numerical methodology for the super-resolution problem for modelable signal space Ω with intrinsic dimension m .

Under the mathematical model we present above, for any modeling pair of Ω , (Θ, \mathcal{P}) , a natural idea is to construct the resolution-enhancing map \mathcal{L} as

$$\mathcal{L} = \mathcal{P}_H \circ \mathcal{P}_L^{-1}, \quad (2.7)$$

where \mathcal{P}_L^{-1} should be understood as the preimage operator.

More precisely, for the noisy measurement given by $y = \mathcal{P}_L(\theta^*) + W$, the numerical methodology contains the following two steps:

1. We estimate the parameter $\hat{\theta}$ by solving the following non-convex optimization problem:

$$\min_{\theta \in \Theta} \varphi(\theta) := \frac{1}{2} \cdot \|\mathcal{P}_L(\theta) - y\|^2. \quad (2.8)$$

2. We obtain resolution-enhanced signal by calculating $\mathcal{P}_H(\hat{\theta})$.

As discussed at the end of Section 2.1, the injection of G_L plays an important role in the uniqueness of the recovered signal. Here, for any modeling pair (Θ, \mathcal{P}) , any solution to the optimization problem (2.8) results in the approximation of the ground truth signal by $\mathcal{P}_L(\hat{\theta})$.

Notice that for chosen modeling pair (Θ, \mathcal{P}) , to ensure the solution of the optimization problem is unique, we need to have the assumption that $2K_L + 1 > \dim(\Theta)$. Under this framework, searching for an appropriate high-resolution signal in \mathcal{H}_H is transformed to search for a suitable parameter in Θ , the dimension reduction is thus achieved.

3 Mathematical Theory for Model-SR

In this section, we develop the fundamental mathematical theory under the model-based super-resolution framework. Section 3.1 is dedicated to introducing the general stability result. The optimization problem is investigated in Section 3.2. Throughout this section, we consider the modelable signal space Ω with intrinsic dimension m and representation pair (Θ, \mathcal{P}) .

3.1 Stability Estimate

Recall that the model map $\mathcal{P} : \Theta \rightarrow \Omega$ is a “local” bijection. We first analyze the local property of the low-resolution map and show the Lipschitz continuity of its inverse.

Theorem 3.1. *Assume that $U \subset \mathbb{R}^m$ is a convex compact set. Consider $\mathcal{P}_L \in C^1(\mathbb{R}^m, \mathcal{H}_L)$ satisfying that*

- $\mathcal{P}_L|_U$ is injective,
- $D\mathcal{P}_L(\theta)$ is injective for all $\theta \in U$.

Then, for every $\theta, \theta' \in U$, there exists $C_U > 0$ such that

$$\|\theta - \theta'\| \leq C_U \cdot \|\mathcal{P}_L(\theta) - \mathcal{P}_L(\theta')\|. \quad (3.1)$$

Further, if $\|D\mathcal{P}_H\|_{op} \leq C'$, then we have

$$\|\mathcal{P}_H(\theta) - \mathcal{P}_H(\theta')\| \leq C'_U \cdot \|\mathcal{P}_L(\theta) - \mathcal{P}_L(\theta')\|, \quad (3.2)$$

where $C'_U = C_U \cdot C'$.

The above theorem is a consequence of Theorem 2.1 [56]. For the sake of completeness and the convenience of readers, we sketch the proof in Appendix 10.1.

Now, consider the noisy low-resolution measurement $y \in \mathbb{C}^{2K_L+1}$ given by

$$y = G_L(\psi) + W = \mathcal{P}_L(\theta^*) + W, \quad (3.3)$$

where $\theta^* \in \Theta$, and $W = (W_{-K_L}, \dots, W_{K_L})$ is the noise vector with $\|W\| < \sigma$. To derive the stability estimate, we first introduce

Definition 4. *Given the low-resolution noisy measurement y , we say $\theta \in \Theta$ is a (Θ, σ) -admissible if*

$$\|\mathcal{P}_L(\theta) - y\| < \sigma. \quad (3.4)$$

Due to the continuity of \mathcal{P} and G_L , the low-resolution map \mathcal{P}_L is continuous. Therefore, the parameter $\hat{\theta}$ that is slightly perturbed from θ^* is also (Θ, σ) -admissible. As a consequence of Theorem 3.1, we have the following Lipschitz stability estimate for (Θ, σ) -admissible parameters.

Corollary 3.2. *Assume that $U \subset \mathbb{R}^m$ is a convex compact set. Consider $\mathcal{P}_L \in C^1(\mathbb{R}^m, \mathcal{H}_L)$ satisfying that*

- $\mathcal{P}_L|_U$ is injective,
- $D\mathcal{P}_L(\theta)$ is injective for all $\theta \in U$,

and $\|D\mathcal{P}_H\|_{op} \leq C$. Let $\hat{\theta} \in U$ be a (Θ, σ) -admissible parameter, then there exists a constant $C' > 0$ such that

$$\|\mathcal{P}_H(\hat{\theta}) - \mathcal{P}_H(\theta^*)\| < C' \cdot \sigma. \quad (3.5)$$

Proof. Notice that

$$\|\mathcal{P}_L(\hat{\theta}) - \mathcal{P}_L(\theta^*)\| \leq \|\mathcal{P}_L(\hat{\theta}) - y\| + \|\mathcal{P}_L(\theta^*) - y\| < 2\sigma. \quad (3.6)$$

By Theorem 3.1, we have

$$\|\mathcal{P}_L(\hat{\theta}) - \mathcal{P}_L(\theta^*)\| \leq C'_U \cdot \|\mathcal{P}_L(\hat{\theta}) - \mathcal{P}_L(\theta^*)\| < 2C'_U \cdot \sigma. \quad (3.7)$$

□

As mentioned in the previous section, modeling Ω using more parameters is always possible. The following corollary generalizes the above stability estimate for a compatible modeling pair $(\tilde{\Theta}, \tilde{\mathcal{P}})$.

Corollary 3.3. *Assume that $U \subset \mathbb{R}^m$ is a convex compact set. Consider $\mathcal{P}_L \in C^1(\mathbb{R}^m, \mathcal{H}_L)$ satisfying that*

- $\mathcal{P}_L|_U$ is injective,
- $D\mathcal{P}_L(\theta)$ is injective for all $\theta \in U$,

and $\|D\mathcal{P}_H\|_{op} \leq C$. Let $\tilde{\theta}^* \in \tilde{\Theta}$ satisfying $\pi_p(\tilde{\theta}^*) = \theta^*$, and $\tilde{\theta}'$ be a $(\tilde{\Theta}, \sigma)$ -admissible parameter, then there exists a constant $C' > 0$ such that

$$\|\tilde{\mathcal{P}}_H(\tilde{\theta}') - \tilde{\mathcal{P}}_H(\tilde{\theta}^*)\| < C' \cdot \sigma. \quad (3.8)$$

Proof. We denote $\hat{\theta} = \pi_p(\tilde{\theta}')$. By definition, we have

$$\tilde{\mathcal{P}}_L(\tilde{\theta}') = G_L \circ \pi_s \circ \tilde{\mathcal{P}}(\tilde{\theta}') = G_L \circ \mathcal{P} \circ \pi_p(\tilde{\theta}') = \mathcal{P}_L(\hat{\theta}),$$

and

$$\tilde{\mathcal{P}}_H(\tilde{\theta}') = G_H \circ \pi_s \circ \tilde{\mathcal{P}}(\tilde{\theta}') = G_H \circ \mathcal{P} \circ \pi_p(\tilde{\theta}') = \mathcal{P}_H(\hat{\theta}).$$

Since $\tilde{\theta}'$ is a $(\tilde{\Theta}, \sigma)$ -admissible parameter, we have

$$\|\tilde{\mathcal{P}}_L(\tilde{\theta}') - y\| = \|\tilde{\mathcal{P}}_L(\tilde{\theta}') - (\tilde{\mathcal{P}}_L(\tilde{\theta}^*) + W)\| < \sigma, \quad (3.9)$$

which implies

$$\|\mathcal{P}_L(\hat{\theta}) - y\| = \|\mathcal{P}_L(\hat{\theta}) - (\mathcal{P}_L(\theta^*) + W)\| < \sigma. \quad (3.10)$$

By Corollary 3.2, we have

$$\|\mathcal{P}_H(\hat{\theta}) - \mathcal{P}_H(\theta^*)\| < C' \cdot \sigma, \quad (3.11)$$

for some constant $C' > 0$. Thus, we conclude that

$$\|\tilde{\mathcal{P}}_H(\tilde{\theta}') - \tilde{\mathcal{P}}_H(\tilde{\theta}^*)\| < C' \cdot \sigma. \quad (3.12)$$

□

The two corollaries above characterize the Lipschitz stability of the resolution-enhancing map. It is worthwhile to point out that in the stability estimate the Lipschitz constant C_U and the bound for $\|D\mathcal{P}_H\|_{op}$ in Theorem 3.1 are of great importance. In addition to the model itself, the former one depends on K_L , and the latter one depends on K_H . The precise characterization of the two quantities reveals the relationship between the stability of the resolution-enhancing map and the super-resolution factor (SRF). However, the analysis on C_U is usually challenging even for concrete models. Based on the stability result given above, we conduct a detailed analysis of three concrete signal models in Section 4, 5 and 6, respectively.

At the end of this section, we add a brief discussion on the case where $\dim \tilde{\Theta} < m$. Unlike the noiseless case, the modeling for Ω using $\tilde{\Theta}$ is possible. A natural question is that for a given noise level when Ω can be modeled using fewer parameters? A typical example is the computational resolution limit problem for line spectral estimation problem, see e.g. [29]. In their research, the authors characterize the gap between the signal generated by n sources and $n - 1$ sources for a given noise level through the minimum separation distance condition.

3.2 The Optimization Problem

In the literature, there are vast numerical methods of optimization to solve the nonlinear least square problem (2.8), see e.g. [57] for a brief survey.

In the following, we characterize the landscape of optimization problem (2.8). We consider the case where (Θ, \mathcal{P}) is a representation pair, and we focus on the local property of $\varphi(\theta)$. Let the noisy low-resolution measurement be given in (3.3). We first write the objective function as

$$\varphi(\theta) = \frac{1}{2} \cdot \|\mathcal{P}_L(\theta) - y\|^2 = \frac{1}{2} \cdot \sum_{k=-K_L}^{K_L} |\mathcal{P}_{L,k}(\theta) - y_k|^2, \quad (3.13)$$

where $y_k = \mathcal{P}_{L,k}(\theta^*) + W_k$. The following theorem shows that for any solution to (2.8), under certain noise level, the objective function is locally ν_l -convex and ν_u -smooth in the neighborhood of the solution.

Theorem 3.4. *Assume that $U \subset \mathbb{R}^m$ is a compact set. Consider $\mathcal{P}_L \in C^2(\mathbb{R}^m, \mathcal{H}_L)$ satisfying that*

- $\mathcal{P}_L|_{\Theta}$ is injective,
- $D\mathcal{P}_L(\theta)$ is injective for all $\theta \in U$.

Let $\hat{\theta} \in U$ be a solution to optimization problem (2.8), then

- $\hat{\theta}$ is (Θ, σ) -admissible.
- there exists a neighborhood of $\hat{\theta}$, say $U_{\hat{\theta}} \subset U \subset \Theta$, and $\nu_u, \nu_l > 0$ such that

$$\nu_l \mathcal{I} \preceq \nabla^2 \varphi(\theta) \preceq \nu_u \mathcal{I}, \quad \forall \theta \in U_{\hat{\theta}}, \quad (3.14)$$

provided $\sigma \leq \frac{\sigma_{\min}^2(D\mathcal{P}_L(\hat{\theta}))}{\|\xi\|}$, where $\xi = (\|\nabla^2 \mathcal{P}_{L,-K_L}\|_{op}, \dots, \|\nabla^2 \mathcal{P}_{L,K_L}\|_{op})$.

Remark 3.5. The (Θ, σ) -admissibility of $\hat{\theta}$ implies the stability estimate (3.5) holds provided that DP_H is bounded. If we consider the modeling pair $(\tilde{\Theta}, \tilde{\mathcal{P}})$, the analogue of admissibility and stability estimate still holds.

Following the standard convergence analysis, the theoretical convergence rate of different optimization algorithms can be derived in this case. For instance, for suitable initialization and step size, gradient descent method has convergence rate $\mathcal{O}\left(\left(1 - \frac{\nu_l}{\nu_u}\right)^t\right)$, and Nesterov accelerated gradient descent has convergence rate $\mathcal{O}\left(\left(1 - \frac{\sqrt{\nu_l}}{\sqrt{\nu_u}}\right)^t\right)$.

4 Point Source Model

In this section, we consider the super-resolution problem for the point source model.

4.1 Preliminary

We consider signals generated by n sources in the interval $[0, 1]_*$ with amplitudes taking values in a closed interval $I \subset [-A_I, A_I]$. Let $\Theta = I^n \times [0, 1]_*^n$ be the parameter space and let $\theta = (\theta_{1,1}, \dots, \theta_{n,1}, \theta_{1,2}, \dots, \theta_{n,2}) \in \Theta$. We define the model map as

$$\mathcal{P}(\theta) = \psi(x) = \sum_{j=1}^n \theta_{j,1} \delta_{\theta_{j,2}}. \quad (4.1)$$

Here, $\theta_{j,2}$ represents the position of the point sources, $\theta_{j,1}$ the corresponding amplitude. The intrinsic dimension of the signal space is $2n$. Then, the signal space has an explicit form:

$$\Omega = \left\{ \sum_{j=1}^n \theta_{j,1} \delta_{\theta_{j,2}} : \theta_{j,1} \in I, \theta_{j,2} \in [0, 1]_* \right\}. \quad (4.2)$$

For the grid defined by $\omega_k = k$, we have

$$g_k = \sum_{j=1}^n \theta_{j,1} e^{-2\pi i \theta_{j,2} k}. \quad (4.3)$$

The low- and high-resolution sampling operators, G_L and G_H , can be defined by (2.2) and (2.3) respectively. Consequently, the noisy low-resolution measurement can be expressed as

$$y_k = g_k + W_k = \sum_{j=1}^n \theta_{j,1} e^{-2\pi i \theta_{j,2} k} + W_k, \quad k = -K_L, \dots, K_L, \quad (4.4)$$

where W_k is the noise term with $|W_k| < \sigma$. We assume that $K_L \geq n$. The Rayleigh length of this system is defined as $RL = \frac{1}{2K_L}$.

4.2 Theoretical Discussion

In this section, we consider signals generated by n different point sources. We assume that $\theta_{j,1} \neq 0$ and $\theta_{j,2}$'s are pairwise different. Otherwise, the signal space has an intrinsic dimension less than $2n$, and one should consider the corresponding representation pair. We have the following theorem on the stability estimate.

Theorem 4.1. *For any given $\theta^* = (\theta_{1,1}^*, \dots, \theta_{n,1}^*, \theta_{1,2}^*, \dots, \theta_{n,2}^*) \in \Theta$, let $\Delta = \frac{1}{2} \cdot \min_{p \neq q} d_{\mathbb{T}}(\theta_{p,2}^*, \theta_{q,2}^*)$, and $U = \prod_{j=1}^n \left(B(\theta_{j,1}^*, \frac{|\theta_{j,1}^*|}{2}) \cap I \right) \times \prod_{j=1}^n B(\theta_{j,2}^*, \Delta)$. Then, there exists $C_U > 0$ such that for any $\theta, \theta' \in \Theta$,*

$$\|\theta - \theta'\| \leq C_U \cdot \|\mathcal{P}_L(\theta) - \mathcal{P}_L(\theta')\|. \quad (4.5)$$

Further, we have

$$\|D\mathcal{P}_H\|_{op}^2 \leq (2K_H + 1)n + \frac{4n\pi^2 A_I^2}{3} \cdot (K_H(K_H + 1)(2K_H + 1)) \triangleq C'^2. \quad (4.6)$$

By letting $C'_U = C_U \cdot C'$, we have

$$\|\mathcal{P}_H(\theta) - \mathcal{P}_H(\theta')\| \leq C'_U \cdot \|\mathcal{P}_L(\theta) - \mathcal{P}_L(\theta')\|. \quad (4.7)$$

As a consequence, if $\hat{\theta} \in U$ be a (Θ, σ) -admissible parameter, then

$$\|\mathcal{P}_H(\hat{\theta}) - \mathcal{P}_H(\theta^*)\| < 2C'_U \cdot \sigma. \quad (4.8)$$

We point out that θ^* in the above theorem can be determined exactly from the low-resolution measurement for the noiseless measurement. This implies that the signal $\mathcal{P}(\theta^*)$ can be exactly recovered. We also notice that the result can be extended to the case when the sources have complex amplitudes. These observations indicate that within the proposed framework, the exact signal recovery does not require minimum separation distance condition nor the conditions on source signs for the noiseless measurement (this is to be contrasted with the BLASSO strategy, for which counter-example exists for sources having arbitrary sign and separation distance below $1RL$ [22]). Further, the stability result offers a perspective on how the ℓ_2 error of high-resolution signal depends on noise.

Remark 4.2. *We notice that the authors derived ℓ_1 version of stability estimates for the total-variation-norm-minimization-based solution to the super-resolution problem of the point source model under the minimum separation condition in [16, 17].*

We point out that the Lipschitz constant C_U in (4.5) depends not only on K_L, K_H but also the minimum separation distance between the sources. We leave the detailed characterization of the Lipschitz constant as the future work. Meanwhile, we expect the theory on computational resolution limit can be included in this framework by analyzing the landscape of objective function $\varphi(\theta)$ defined in (2.8).

5 Signals with Finite Rate of Innovation

In this section, we consider the super-resolution problem for signals with a finite rate of innovation (FRI), see e.g. [58, 59]. We use signals generated by derivatives of Diracs in the physics domain as a typical example for demonstration.

We consider the sources in the interval $[0, 1)$ with amplitudes taking values in a closed interval $I \subset [-A_I, A_I]$. For the sources corresponding to the r -th derivative of delta, $r = 0, \dots, R$, we denote the total number as n_r , the source positions as $\{\theta_{r,j,2}\}_{j=1}^{n_r}$, and the amplitudes as $\{\theta_{r,j,1}\}_{j=1}^{n_r}$. We write $N = \sum_{r=0}^R n_r$ for the total number of sources.

Let $\Theta = I^N \times [0, 1]_*^N$ be the parameter space, we define the model map as

$$\mathcal{P}(\theta) = \psi(x) = \sum_{r=0}^R \sum_{j=1}^{n_r} \theta_{r,j,1} \delta_{\theta_{r,j,2}}^{(r)}, \quad (5.1)$$

where $\theta = (\theta_{1,0,1}, \dots, \theta_{n_R,R,1}, \theta_{1,0,2}, \dots, \theta_{n_R,R,2})$, and $\delta^{(r)}$ denotes the r -th derivative of δ . Thus, the signal space can be written as $\Omega = \mathcal{P}(\Theta)$. For the grid $\omega_k = k$, we have

$$g_k = \sum_{r=0}^R \sum_{j=1}^{n_r} \theta_{r,j,1} \cdot (-2\pi i k)^r e^{-2\pi i \theta_{r,j,2} k}. \quad (5.2)$$

The low- and high-resolution sampling operators, G_L and G_H , are defined by (2.2) and (2.3) respectively. Consequently, the noisy low-resolution measurement can be expressed as

$$y_k = g_k + W_k = \sum_{r=0}^R \sum_{j=1}^{n_r} \theta_{r,j,1} \cdot (-2\pi i k)^r e^{-2\pi i \theta_{r,j,2} k} + W_k, \quad k = -K_L, \dots, K_L, \quad (5.3)$$

where W_k is the noise term with $|W_k| < \sigma$. We assume that $K_L \geq N$. The Rayleigh length is defined as $RL = \frac{1}{2K_L}$.

Applying Theorem 3.1 and Corollary 3.2 to this model, we have the following stability estimate.

Theorem 5.1. *For any given $\theta^* = (\theta_{0,1,1}^*, \dots, \theta_{R,n_R,1}^*, \theta_{0,1,2}^*, \dots, \theta_{R,n_R,2}^*) \in \Theta$, let $\Delta_r = \frac{1}{2} \cdot \min_{p \neq q} d_{\mathbb{T}}(\theta_{r,p,2}^*, \theta_{r,q,2}^*)$. We assume that $\theta_{r,j,1}^* \neq 0$, for $j = 1, \dots, n_r$ and $r = 0, \dots, R$, and $\Delta_r > 0$. Let $U = \prod_{r=0}^R \prod_{j=1}^{n_r} \left(B(\theta_{r,j,1}^*, \frac{|\theta_{r,j,1}^*|}{2}) \cap I \right) \times \prod_{r=0}^R \prod_{j=1}^{n_r} B(\theta_{r,j,2}^*, \Delta_r)$. Then, there exists $C_U > 0$ such that for any $\theta, \theta' \in \Theta$,*

$$\|\theta - \theta'\| \leq C_U \cdot \|\mathcal{P}_L(\theta) - \mathcal{P}_L(\theta')\|. \quad (5.4)$$

Furthermore, we have

$$\|\overline{D\mathcal{P}_H}\|_{op}^2 \leq \sum_{k=-K_L}^{K_L} \sum_{r=0}^R n_r (2\pi k)^{2r} (1 + 4\pi^2 k^2 A_I^2) \triangleq C'^2. \quad (5.5)$$

By letting $C'_U = C_U \cdot C'$, we have

$$\|\mathcal{P}_H(\theta) - \mathcal{P}_H(\theta')\| \leq C'_U \cdot \|\mathcal{P}_L(\theta) - \mathcal{P}_L(\theta')\|. \quad (5.6)$$

As a consequence, if $\hat{\theta} \in U$ is a (Θ, σ) -admissible parameter, then

$$\|\mathcal{P}_H(\hat{\theta}) - \mathcal{P}_H(\theta^*)\| < 2C'_U \cdot \sigma. \quad (5.7)$$

Remark 5.2. The assumption $\theta_{r,j,1}^* \neq 0$ is for the ease of presentation. One can relax this assumption to $(\theta_{0,1,1}^*, \dots, \theta_{R,n_R,1}^*) \neq 0$ and get similar result. It coincides with considering the signal subspace corresponding to fewer sources.

As a generalization of the point source model, there are few theoretical results for signals with a finite rate of innovation. We notice that the authors consider the resolution limit problem from the optimal construction perspective for $R = 1$ in [33]. For the general model, the problem is still widely open. To our knowledge, characterizing the resolution limit for FRI signals is also an open problem.

6 Towards General Signals

The previous two sections consider the super-resolution problem for signals having discrete forms in the physical domain. In this section, we consider continuous signals in the physical domain.

To demonstrate the idea, we consider signals that are probability density functions of Gaussian mixtures with n components. More precisely, let $\Theta = I_1^n \times I_2^n \times [0, 1]_*^n$ be the parameter space. We define the model map as

$$\mathcal{P}(\theta) = \psi(x) = \sum_{j=1}^n \theta_{j,1} \exp\left\{-\frac{(x - \theta_{j,3})^2}{2\theta_{j,2}^2}\right\} \quad (6.1)$$

where $\theta = (\theta_{1,1}, \dots, \theta_{n,1}, \theta_{1,2}, \dots, \theta_{n,2}, \theta_{1,3}, \dots, \theta_{n,3})$. Here $\theta_{j,1}$, $\theta_{j,2}$ and $\theta_{j,3}$ are the weight, variance and mean of the j -th component, and they take values in a closed interval I_1 , a closed interval of positive real numbers I_2 , and $[0, 1]_*$, respectively. The signal space can be written as $\Omega = \mathcal{P}(\Theta)$. For the grid $\omega_k = k$, we have

$$g_k = \sqrt{2\pi} \cdot \sum_{j=1}^n \theta_{j,1} \theta_{j,2} \cdot e^{-2\pi i \theta_{j,3} \omega_k} \cdot e^{-2\pi^2 \theta_{j,2}^2 \omega_k^2}. \quad (6.2)$$

The low- and high-resolution sampling operators, G_L and G_H , are defined by (2.2) and (2.3) respectively. Consequently, the noisy low-resolution measurement can be expressed as

$$y_k = g_k + W_k = \sqrt{2\pi} \cdot \sum_{j=1}^n \theta_{j,1} \theta_{j,2} \cdot e^{-2\pi i \theta_{j,3} \omega_k} \cdot e^{-2\pi^2 \theta_{j,2}^2 \omega_k^2} + W_k, \quad k = -K_L, \dots, K_L, \quad (6.3)$$

where W_k is the noise term with $|W_k| < \sigma$. We assume that $2K_L + 1 \geq 3n$.

We have the following theorem for the stability estimate of the super-resolution problem.

Theorem 6.1. For any given $\theta^* = (\theta_{1,1}^*, \dots, \theta_{n,1}^*, \theta_{1,2}^*, \dots, \theta_{n,2}^*, \theta_{1,3}^*, \dots, \theta_{n,3}^*) \in \Theta$, let $\Delta = \frac{1}{2} \cdot \min_{p \neq q} d_{\mathbb{T}}(\theta_{p,3}^*, \theta_{q,3}^*)$. We assume that $\theta_{j,1}^* \neq 0$ for $j = 1, \dots, n$ and $\Delta > 0$. Let $U = \prod_{j=1}^n \left(B(\theta_{j,1}^*, \frac{|\theta_{j,1}^*|}{2}) \cap I_1 \right) \times \prod_{j=1}^n \left(B(\theta_{j,2}^*, \frac{|\theta_{j,2}^*|}{2}) \cap I_2 \right) \times \prod_{j=1}^n B(\theta_{j,3}^*, \Delta)$. Then, there exists $C_U > 0$ such that for any $\theta, \theta' \in \Theta$,

$$\|\theta - \theta'\| \leq C_U \cdot \|\mathcal{P}_L(\theta) - \mathcal{P}_L(\theta')\|. \quad (6.4)$$

Furthermore,

$$\|D\mathcal{P}_H\|_{op} \leq C', \quad (6.5)$$

where C' does not depend on K_H . By letting $C'_U = C_U \cdot C'$, we have

$$\|\mathcal{P}_H(\theta) - \mathcal{P}_H(\theta')\| \leq C'_U \cdot \|\mathcal{P}_L(\theta) - \mathcal{P}_L(\theta')\|. \quad (6.6)$$

As a consequence, if $\hat{\theta} \in U$ is a (Θ, σ) -admissible parameter, then

$$\|\mathcal{P}_H(\hat{\theta}) - \mathcal{P}_H(\theta^*)\| < 2C'_U \cdot \sigma. \quad (6.7)$$

Remark 6.2. The assumption $\Delta > 0$ is for the ease of presentation. The above theorem holds as long as $(\theta_{p,2}, \theta_{p,3}) \neq (\theta_{q,2}, \theta_{q,3})$ for $p \neq q$.

We note that there is few studies on the super-resolution problems for signals with continuous profiles in the physics space. From the results in Section 3, we observe that appropriate modeling leads to a stable solution to the super-resolution problem. However, for general signals, choosing an appropriate model is challenging. Whether using a physics-based or a data-driven-based model remains a topic worthy of exploration.

7 Numerical Experiments

In this section, we conduct numerical experiments to test the numerical behavior of the proposed method on different signal models. Throughout this section, we define the signal-to-noise ratio for the low-resolution signal as

$$\text{SNR} := 10 \cdot \log_{10} \frac{\|\text{signal}\|}{\|\text{noise}\|}. \quad (7.1)$$

Moreover, all the algorithms to solve the nonlinear least-square problem are based on the Nesterov accelerated gradient descent method.

7.1 Point Source Model

In this section, we conduct two groups of experiments to test the numerical behavior of the proposed numerical scheme for the point source model.

First, we test the stability. We fix $K_L = 10$, then the corresponding Rayleigh length is given by $RL = \frac{1}{20}$. We set 5 groups of point sources aligned in $[0, 1)$ in the following way.

The point sources are separated by $1RL$ in each group, and different groups are separated by $3RL$. We set the amplitude of the sources to follow the uniform distribution $\mathcal{U}[1, 2]$, and the SNR to be around 20. We conduct 20 random experiments where the randomness is from the amplitudes and noise. In each experiment, we pick the initial guess of the source positions by perturbing $0.4RL$ to the ground truth of source positions. Figure 4 shows the numerical result of the above experiments with average SNR = 19.18.

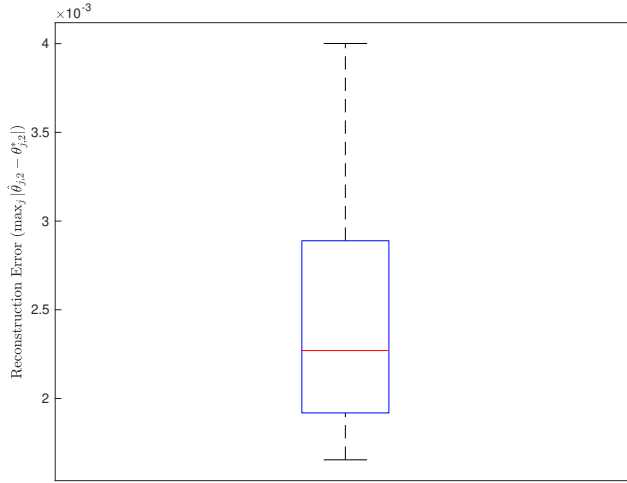


Figure 4: Boxplot of point source position reconstruction error.

To visualize the resolution-enhanced signal in the physics domain, we use the last experiment above. For given super-resolution factors $SRF = 10, 20$, we first extrapolate the high-frequency data according to the reconstructed source positions and amplitudes and then calculate the signal profile in the physics domain by inverse FFT (iFFT), the result is shown in Figure 5.

Second, we demonstrate that the proposed method does not need the separation condition for the noiseless source reconstruction. We fix $K_L = 5$, then the corresponding Rayleigh length is given by $RL = \frac{1}{10}$. We set two point sources in $[0, 1)$ with separation distance $\frac{1}{100}RL$, and set the amplitude of the sources to follow the uniform distribution $\mathcal{U}[1, 2]$. We pick the initial guess of the source position as the ground truth with perturbation half of the separation distance. We stop the algorithm when the residue is at the level $\mathcal{O}(10^{-7})$. Figure 6 shows that the proposed method can distinguish the two point sources and give a good estimation.

7.2 Signals with Finite Rate of Innovation

In this section, we conduct experiments on the proposed numerical scheme for signals with a finite rate of innovation.

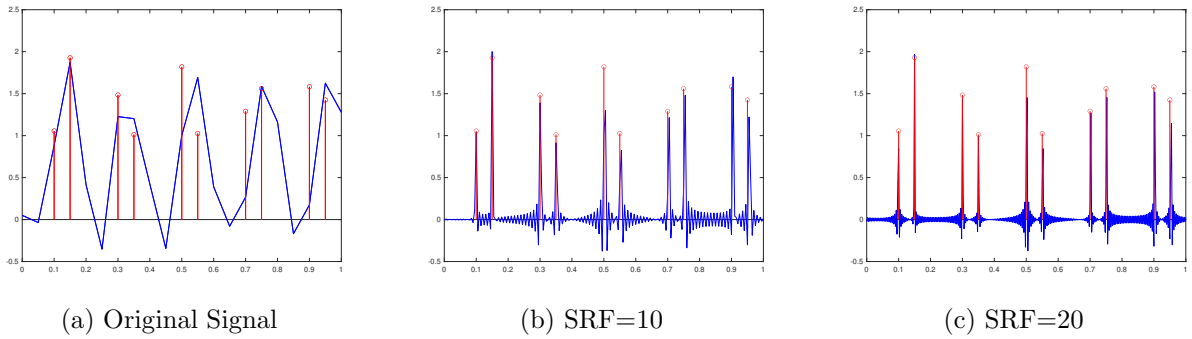


Figure 5: Original signals and resolution enhanced signals in physics domain. The red line represents the ground truth of the point source. The blue line shows the signal profile calculated by iFFT using the original/extrapolated Fourier data. The SNR of the experiment is 20.08.

In the numerical experiment, we fix $K_L = 10$. The corresponding Rayleigh length is $RL = \frac{1}{20}$. The noiseless signal has the form

$$\psi(x) = \sum_{j=1}^5 a_j \delta_{x_j} + \sum_{j=1}^2 b_j \delta'_{y_j} + c \delta''_z, \quad (7.2)$$

where $(x_1, \dots, x_5) = (0.1, 0.15, 0.45, 0.55, 0.9)$, $(y_1, y_2) = (0.7, 0.8)$, $z = 0.3$. Thus, the separation distance between different sources ranges from $1RL$ to $3RL$. We call the source having the form δ_{x_j} as the monopole source, having the form δ'_{y_j} as the dipole source and δ''_z as the quadrupole source. We choose amplitude $a_j \sim \mathcal{U}[1, 2]$ for monopole sources. We choose b_j 's and c by ensuring that signals generated by different types of sources have comparable low-resolution signals in ℓ_2 norm. We conduct 20 random experiments. In each experiment, we pick the initial guess of the source positions by perturbing $0.4RL$ to their ground truth. Figure 7 shows the reconstruction result for the experiment with average SNR = 32.03.

In Figure 7, we observe that the absolute position reconstruction error of the quadrupole source is relatively small. This is because the loss function, especially its high-frequency part, is more sensitive to the higher-order poles.

To visualize the resolution-enhanced signal in the physics domain, we introduce the Dirichlet kernel

$$D_K(x) = \sum_{k=-K}^K e^{2\pi i k x}. \quad (7.3)$$

The convolution of the derivative of Dirac with Dirichlet kernel with increasing K_L leads to

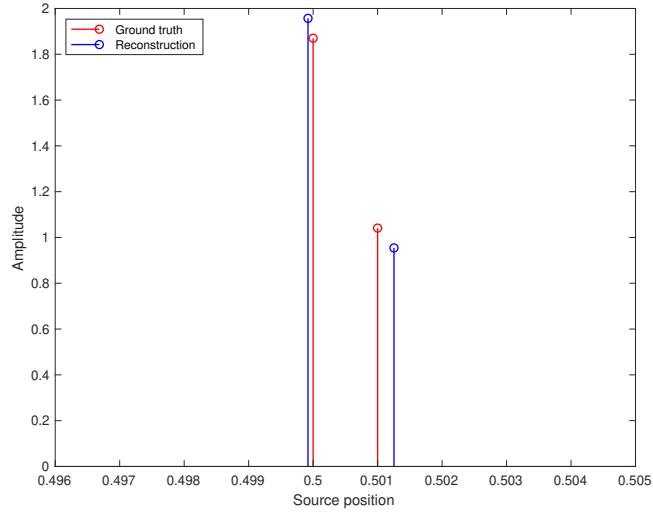


Figure 6: Reconstruction for closely positioned point sources.

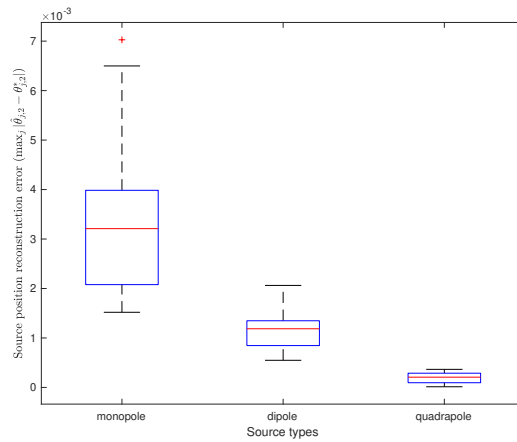


Figure 7: Boxplot of source positions reconstruction error for different types of sources.

the significant amplification of the signal strength. More precisely

$$D_K(x) * \delta^{(r)}(x) = \sum_{k=-K}^K (2\pi i k)^r e^{2\pi i k x}. \quad (7.4)$$

Therefore different order of Diracs generate signals of different amplitudes in the physics domain. We plot these different types of signals in the physics domain in different pictures, see Figure 8. In the Figure, the ground truth for $r \geq 1$ is generated by convoluting the ground truth derivatives of Diracs with the corresponding Dirichlet kernel.

The experiment results demonstrate a stable reconstruction of the source positions. Meanwhile, we observe that the extrapolation in the frequency domain results in reliable resolution-enhanced signals in the physics domain.

7.3 General Signals

We conduct numerical experiments for more complicated signals. In the physics domain, we assume that the signal is a linear combination of components having the following form

$$c(x; \boldsymbol{\mu}) = e^{i(\mu_0 x^2 + \mu_1 x + \mu_2)} \cdot e^{-\frac{(x - \mu_3)^2}{2\mu_4^2}}, \quad (7.5)$$

where $\mu_0, \mu_1, \mu_2 \in \mathbb{R}$, $\mu_3 \in [0, 1)$, $\mu_4 \in (0, \infty)$. Then, the signal can be written as

$$\psi(x) = \sum_{j=1}^n b_j c(x; \boldsymbol{\mu}_j).$$

Suppose we have low-frequency data in the frequency domain and aim to recover the high-frequency data to achieve super-resolution.

The experiment considers a signal having 4 components with different $\boldsymbol{\mu}$'s. Write the signal in the following equivalent form

$$\psi(x) = \sum_{j=1}^4 (\kappa_{0,j} + \kappa_{1,j} i) \cdot e^{i(\kappa_{2,j} x^2 + \kappa_{3,j} x)} \cdot e^{-\frac{(x - \kappa_{4,j})^2}{2\kappa_{5,j}^2}}.$$

Notice that different from the signal models in Section 7.1 and 7.2, we do not have the explicit form of the Fourier transform for the signal above. In the experiment, we set $(\kappa_{4,1}, \kappa_{5,1}) = (0.2, 0.02)$, $(\kappa_{4,2}, \kappa_{5,2}) = (0.4, 0.03)$, $(\kappa_{4,3}, \kappa_{5,3}) = (0.6, 0.01)$, and $(\kappa_{4,4}, \kappa_{5,4}) = (0.8, 0.01)$. In the physical space $[0, 1)$, we setup a grid $\{x_t^{(c)}\}$, defined by $x_t^{(c)} = \frac{t}{127}$, $t = 0, \dots, 127$, for the calculation of FFT. Using this grid, we generate 32 noisy low-frequency data. Then, the associated grid in $[0, 1)$, $\{x_t^{(o)}\}$, has step size $\frac{1}{31}$. We solve the parameters $\{\kappa_{p,q}\}$ by the low-frequency data and draw the picture of the signal on two finer grids having step size $\frac{1}{127}$ and $\frac{1}{4095}$ respectively. We pick the initial guess of $\kappa_{4,j}$ by adding or minus a

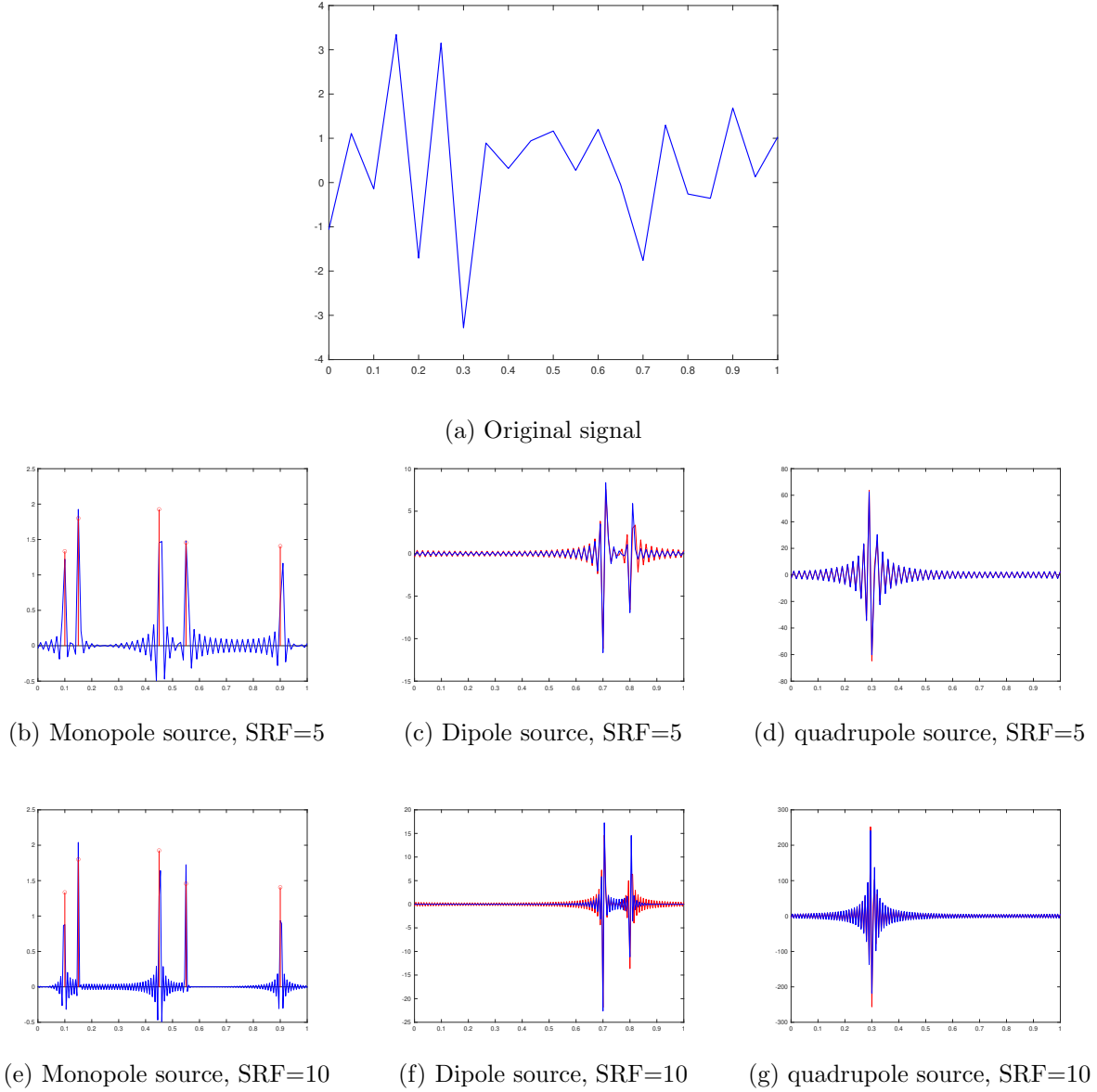


Figure 8: Original signal and resolution-enhanced signals in physics domain. The blue line in all figures shows the signal profile calculated by iFFT using the original/extrapolated Fourier data. The red line in Figure 8b and Figure 8e shows the ground truth of point sources. The red line in Figure 8c, Figure 8f, Figure 8d and Figure 8g shows the signal profile of the ground truth higher pole sources sampled by corresponding Dirichlet kernel. The SNR of the experiment is 30.16.

constant around 0.07 to the ground truth (noticing that the $RL = \frac{1}{32}$ for the system). Consequently, the initial guess for $\kappa_{4,1}$ has error $3.5\kappa_{5,1}$, the initial guess for $\kappa_{4,2}$ has error more than $2\kappa_{5,2}$, and the initial guess for $\kappa_{4,3}$ and $\kappa_{4,4}$ has error $7\kappa_{5,3}$. During the optimization, we restrict $\kappa_{4,j}$ to $(0, 1)$ by re-initialization if $\kappa_{4,j} \notin (0, 1)$ in some step. We visualize the signals in the physics domain, see Figure 9. The original signal is calculated from the iFFT of the

noisy low-frequency samples. The resolution-enhanced signals are calculated by the interpolation of the recovered signal profile. The experiment is conducted under $\text{SNR} = 11.35$.

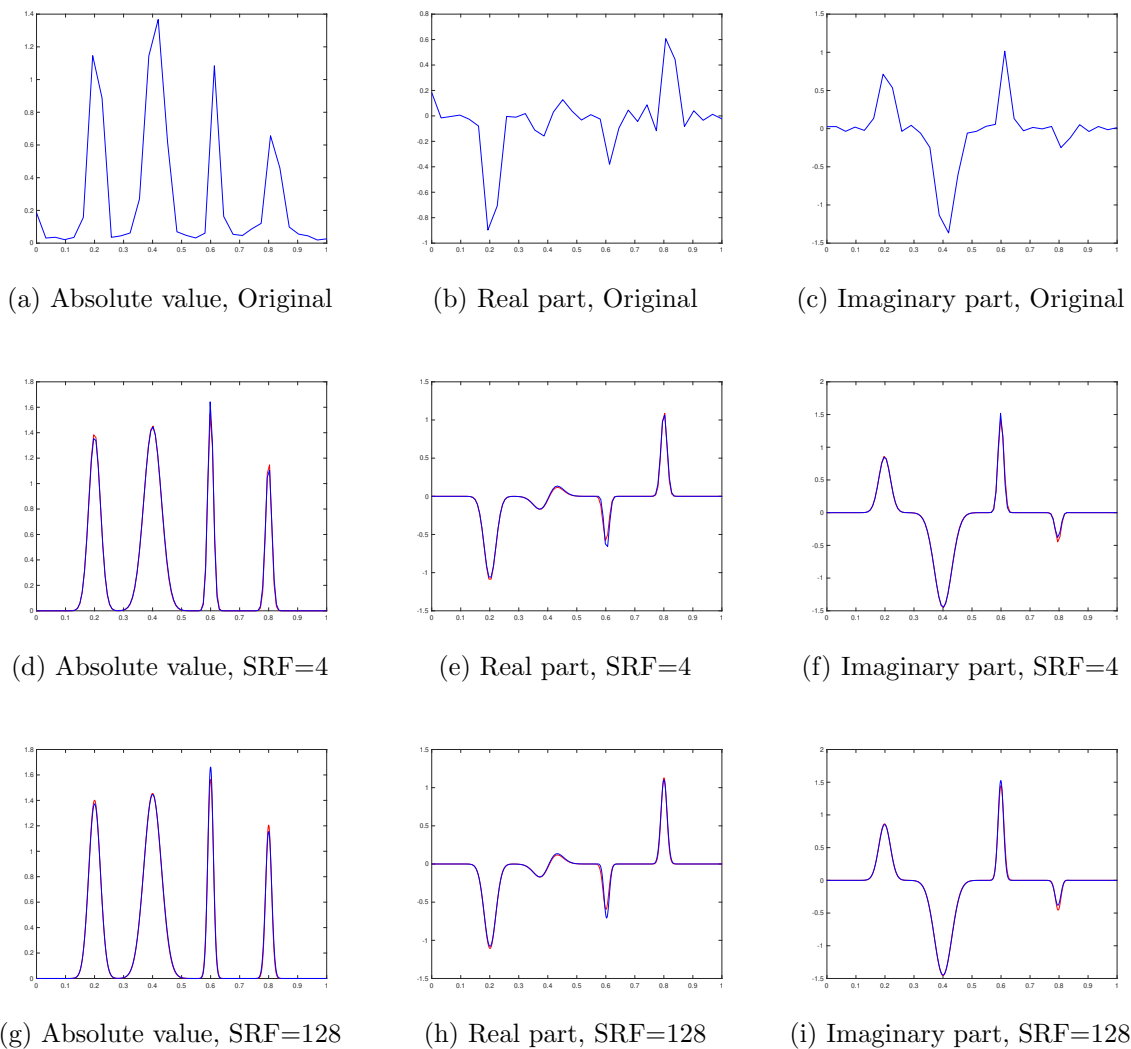


Figure 9: Original signals and resolution enhanced signals in physics domain. The red line represents the ground truth and the reconstructed ones are shown in blue. We define the super-resolution factor (SRF) in the physics domain as the quotient of the two grid point numbers. The first row shows the original signal. The second and third rows show the resolution-enhanced signal with $\text{SRF} = 4$ and 10 respectively. The first column is the absolute value of the signal profile, and the second and third columns are the real and imaginary parts of the signal respectively. The SNR of the experiment is 11.35 .

Notice that using a finer grid of the physics domain to calculate FFT gives a more accurate approximation of the Fourier transform but at the expense of higher computational cost since the Fourier transform is executed in each iteration for the optimization problem.

Finally, we point out that the signal profile used in this experiment is smooth and thus has a rapidly decaying Fourier transform. Therefore, the high-frequency data is very noisy, and the low-frequency data plays an important role in the parameter estimation.

8 Extension

In this section, we discuss several extensions of the model-based super-resolution framework to other problems with similar structures.

8.1 Data Completion

For a typical data completion problem, the sampling grid is slightly different from the one used in the super-resolution problem. We denote the full grid as $\mathcal{M}_F = \{\omega_k\}_{k \in \Lambda}$ and the partial grid as $\mathcal{M}_P = \{\omega_k\}_{k \in \Lambda'}$, where $\Lambda' \subset \Lambda$. For $\Omega \subset C(\mathbb{R})$, we can similarly define the partial sampling operator G_P and full sampling operator G_F as low- and high-resolution sampling operators respectively. Following the routine as in Section 2.1, the model-based data completion framework can be developed. See the following Figure 10 for illustration. In the figure, \mathcal{Q} is the downsampling operator and \mathcal{L} sampling lifting operator satisfying the conditions (2.4) and (2.5). Further, once the suitable modeling pair (Θ, \mathcal{P}) is determined, the numerical methodology and theoretical estimates also apply to the model-based data completion framework.

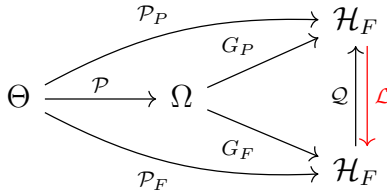


Figure 10: Model-based data completion framework

8.2 Deep Learning

As seen in the previous sections, to achieve super-resolution, we need prior information about the modeling pair (Θ, \mathcal{P}) , especially the model map. For natural images, this is hard even for simple objects. The deep learning-based SISR resolves this issue by approximating the resolution-enhancing map \mathcal{L} via hidden layers.

For generative models, one of the key concepts is the latent space, which is used to represent the signal. The representation captures the intrinsic structure of the signal which lies in a high-dimensional space. The crucial step is to learn the map from the latent space to the signal space. The Model-SR has a similar structure. The parameter space Θ acts as an analogy to the latent space and Ω is signal space that is embedded in high (even infinity) dimensional space. The model map \mathcal{P} is the bridge between the latent and signal space. Thus, the learning step in generative models can be interpreted as finding (an approximation of)

a model map for the signal space.

The connection between Model-SR and deep learning is bi-directional. For one thing, the theory behind Model-SR can offer a perspective and a starting point toward understanding deep learning. For another, deep learning can help find efficient representation/modeling for specific inverse problems.

9 Conclusion

In this paper, we develop the theory of the model-based super-resolution framework. We present the general mathematical theory along with concrete examples and numerical experiments. We show that under suitable modeling, super-resolution problems enjoy certain stability.

Within the proposed framework, the challenging part is the non-convexity nature of the objective function, for which good initial guesses are needed for the convergence of gradient descent algorithms. Efficient methods for selecting good initial guesses in each concrete model shall be studied, and we leave it as future work. The model-based framework can be generalized to other problems. We expect that the results shown in this paper offer another perspective on the super-resolution problem and take a step forward in understanding model-based problems and problems having a similar structure.

10 Appendix

10.1 Proof of Theorem 3.1

If U is a singleton, the result is trivial. We assume that $\text{diam } U := \sup\{\|\theta - \theta'\| : \theta, \theta' \in U\} > 0$, and it is clear that $\text{diam } U < \infty$ since U is compact.

Step 1. Large distance case

For any given $r > 0$, we consider the set $S := \{(\theta, \theta') \in U \times U : \|\theta - \theta'\| \geq r\}$. If S is empty, then it is trivial. Otherwise, notice that S is compact and the map $(\theta, \theta') \mapsto \|\mathcal{P}_L(\theta) - \mathcal{P}_L(\theta')\|$ is continuous, we can then define

$$C_1 := \min\{\|\mathcal{P}_L(\theta) - \mathcal{P}_L(\theta')\| : (\theta, \theta') \in S\}.$$

The injectivity of \mathcal{P}_L guarantees that $C_1' > 0$, and we have

$$\|\theta - \theta'\| \leq C_U \cdot \|\mathcal{P}_L(\theta) - \mathcal{P}_L(\theta')\|, \quad (10.1)$$

with $C_U = \frac{\text{diam } U}{C_1}$.

Step 2. Short distance case

We assume that $\theta, \theta' \in U$ satisfying $\|\theta - \theta'\| \leq r_U$ for some $r_U > 0$ to be determined later. Let $\gamma(t)$ be the line segment defined by $\gamma(t) = (1-t)\theta + t\theta' \in U$, $t \in [0, 1]$. By the convexity of U , we have $\gamma(t) \in U$ for all $t \in [0, 1]$. Combining the fundamental theorem of calculus and $\mathcal{P}_L \in C^1(\mathbb{R}^m, \mathcal{H}_L)$, we can write

$$\mathcal{P}_L(\theta') - \mathcal{P}_L(\theta) = \int_0^1 D(\mathcal{P}_L \circ \gamma)(t) dt = \int_0^1 D\mathcal{P}_L(\gamma(t))(\theta' - \theta) dt.$$

Therefore,

$$D\mathcal{P}_L(\theta)(\theta - \theta') = \mathcal{P}_L(\theta) - \mathcal{P}_L(\theta') + \int_0^1 [D\mathcal{P}_L(\theta) - D\mathcal{P}_L(\gamma(t))] (\theta - \theta') dt,$$

and further we have

$$\|D\mathcal{P}_L(\theta)(\theta - \theta')\| \leq \|\mathcal{P}_L(\theta) - \mathcal{P}_L(\theta')\| + \int_0^1 \|D\mathcal{P}_L(\theta) - D\mathcal{P}_L(\gamma(t))\|_{op} \cdot \|\theta - \theta'\| dt.$$

By rearrangement and straightforward estimation, we have

$$\frac{\|\mathcal{P}_L(\theta) - \mathcal{P}_L(\theta')\|}{\|\theta - \theta'\|} \geq \inf_{z \in \mathbb{S}^{m-1}} \{\|D\mathcal{P}_L(\theta)z\|\} - \sup_{t \in [0, 1]} \|D\mathcal{P}_L(\theta) - D\mathcal{P}_L(\gamma(t))\|_{op}, \quad (10.2)$$

which holds for any $\theta, \theta' \in U$ satisfying $\|\theta - \theta'\| \leq r_U$, where \mathbb{S}^{m-1} is the unit sphere. We then show the right-hand side of (10.2) is bounded below away from 0.

The injectivity of $D\mathcal{P}_L(\theta)$ in U as well as the compactness of U and \mathbb{S}^{m-1} yield that

$$C_2 := \inf_{\theta \in U, z \in \mathbb{S}^{m-1}} \|D\mathcal{P}_L(\theta)z\| > 0.$$

On the other hand, since $\mathcal{P}_L \in C^1(\mathbb{R}^m, \mathcal{H}_L)$, U is compact, and $\gamma(t) \in U$ for any $t \in [0, 1]$, there exists a non-decreasing modulus of continuity $\omega_{D\mathcal{P}_L, U}$ such that

$$\|D\mathcal{P}_L(\theta) - D\mathcal{P}_L(\gamma(t))\|_{op} \leq \omega_{D\mathcal{P}_L, U}(\|\theta - \gamma(t)\|) \leq \omega_{D\mathcal{P}_L, U}(\|\theta - \theta'\|) \leq \omega_{D\mathcal{P}_L, U}(r_U),$$

for every $t \in [0, 1]$.

Then, by choosing a sufficient small $r_U > 0$ such that $\omega_{D\mathcal{P}_L, U}(r) \leq \frac{C_2}{2}$, we have

$$\|\theta - \theta'\| \leq C_U \cdot \|\mathcal{P}_L(\theta) - \mathcal{P}_L(\theta')\|, \quad (10.3)$$

with $C_U = \frac{2}{C_2}$.

Step 3.

Using the convexity of U , it is straightforward that if $\|D\mathcal{P}_L(\theta)\| \leq C'$ for all $\theta \in U$, then

$$\|\mathcal{P}_H(\theta) - \mathcal{P}_H(\theta')\| \leq C' \cdot \|\theta - \theta'\| \leq C_U \cdot C' \cdot \|\mathcal{P}_L(\theta) - \mathcal{P}_L(\theta')\|. \quad (10.4)$$

10.2 Proof of Theorem 3.4

Step 1.

let $\hat{\theta} \in U$ be a solution to (2.8), we have

$$\|\mathcal{P}_L(\hat{\theta}) - y\| \leq \|\mathcal{P}_L(\theta^*) - y\| = \|W\| < \sigma. \quad (10.5)$$

Hence, $\hat{\theta}$ is (Θ, σ) -admissible.

Step 2.

Straightforward calculation gives

$$\begin{aligned} \nabla\varphi(\theta) &= \operatorname{Re}\{\overline{D\mathcal{P}_L}^\top (\mathcal{P}_L(\theta) - y_k)\}, \\ \nabla^2\varphi(\theta) &= \operatorname{Re}\{\overline{D\mathcal{P}_L}^\top D\mathcal{P}_L + \mathcal{N}(\theta)\}, \end{aligned}$$

where $\mathcal{N}(\theta) = \sum_{k=-K_L}^{K_L} (\mathcal{P}_{L,k}(\theta) - y_k) \cdot \nabla^2 \overline{\mathcal{P}}_{L,k}$.

By the assumption that $\mathcal{P}_L \in C^2(\mathbb{R}^m, \mathcal{H}_L)$ and U is compact, there exists $A > 0$, s.t. $\|\overline{D\mathcal{P}_L}^\top D\mathcal{P}_L\| \leq A$ and $\|\nabla^2 \mathcal{P}_{L,k}\|_{op} \leq A$, for $k = -K_L, \dots, K_L$. Then, it is clear that there exists $\nu_u > 0$, s.t. $\nabla^2\varphi(\theta) \preceq \nu_u \mathcal{I}$, $\forall \theta \in U$.

By the assumption that $D\mathcal{P}_L(\theta)$ is injective for all $\theta \in U$, the matrix $\overline{D\mathcal{P}_L(\hat{\theta})}^\top D\mathcal{P}_L(\hat{\theta})$ is positive definite, which implies $\sigma_{\min}(D\mathcal{P}_L(\hat{\theta})) > 0$. Let $\xi = (\|\nabla^2 \mathcal{P}_{L,-K_L}\|_{op}, \dots, \|\nabla^2 \mathcal{P}_{L,K_L}\|_{op})$. Notice that,

$$\begin{aligned} \|\mathcal{N}(\hat{\theta})\|_{op} &\leq \sum_{k=-K_L}^{K_L} \left| \mathcal{P}_{L,k}(\hat{\theta}) - y_k \right| \|\nabla^2 \overline{\mathcal{P}}_{L,k}\|_{op} \\ &\leq \left(\sum_{k=-K_L}^{K_L} \left| \mathcal{P}_{L,k}(\hat{\theta}) - y_k \right|^2 \right)^{1/2} \cdot \|\xi\| \\ &< \|\xi\| \cdot \sigma. \end{aligned} \quad (10.6)$$

By Weyl's theorem, we have

$$\begin{aligned} \lambda_{\min} \left(\overline{D\mathcal{P}_L(\hat{\theta})}^\top D\mathcal{P}_L(\hat{\theta}) + \mathcal{N}(\hat{\theta}) \right) &\geq \lambda_{\min} \left(\overline{D\mathcal{P}_L(\hat{\theta})}^\top D\mathcal{P}_L(\hat{\theta}) \right) - \|\mathcal{N}(\hat{\theta})\|_{op} \\ &> \sigma_{\min}^2 \left(D\mathcal{P}_L(\hat{\theta}) \right) - \|\xi\| \cdot \sigma \geq 0. \end{aligned}$$

Therefore, the matrix $\overline{D\mathcal{P}_L(\hat{\theta})}^\top D\mathcal{P}_L(\hat{\theta}) + \mathcal{N}(\hat{\theta})$ is positive definite and so is $\nabla^2\varphi(\hat{\theta})$. Since $\nabla^2\varphi(\theta)$ depends continuously on θ , there exists a closed neighborhood $U_{\hat{\theta}} \subset U$, such that $\nabla^2\varphi(\theta)$ is positive definite for all $\theta \in U_{\hat{\theta}}$. The proof is finished by taking

$$\nu_l = \inf_{\theta \in U_{\hat{\theta}}} \lambda_{\min}(\nabla^2\varphi(\theta)).$$

10.3 Proof of Theorem 4.1

We notice that U is compact and convex. According to Theorem 3.1, we only need to verify $\mathcal{P}_L|_U$ is injective and $D\mathcal{P}_L(\theta)$ is injective for all $\theta \in U$.

Step 1. Injectivity of $\mathcal{P}_L|_U$:

For $\theta, \theta' \in U$, we assume that $\mathcal{P}_L(\theta) = \mathcal{P}_L(\theta')$, i.e.

$$\sum_{j=1}^n \theta_{j,1} e^{-2\pi i \theta_{j,2} k} = \sum_{j=1}^n \theta'_{j,1} e^{-2\pi i \theta'_{j,2} k} \quad |k| \leq K_L. \quad (10.7)$$

By the choice of Δ , $\theta_{2,p}^* \notin B(\theta_{2,q}^*, \Delta)$, for $p \neq q$. Without loss of generality, we suppose $\theta_{1,2} = \theta'_{1,2}, \dots, \theta_{s,2} = \theta'_{s,2}$. Denote $\phi_{K_L}(\theta_{j,2}) = e^{2\pi i \theta_{j,2} K_L} \cdot (1, e^{-2\pi i \theta_{j,2}}, \dots, e^{-4\pi i \theta_{j,2} K_L})^\top$, and define $A_\theta = (\phi_{K_L}(\theta_{1,2}), \dots, \phi_{K_L}(\theta_{s,2}), \phi_{K_L}(\theta_{s+1,2}), \dots, \phi_{K_L}(\theta_{n,2}), \phi_{K_L}(\theta'_{s+1,2}), \dots, \phi_{K_L}(\theta'_{n,2}))$, $\phi_\theta = (\theta_{1,1} - \theta'_{1,1}, \dots, \theta_{s,1} - \theta'_{s,1}, \theta_{s+1,1}, \dots, \theta_{n,1}, \theta'_{s+1,1}, \dots, \theta'_{n,1})^\top$. We rewrite the equations (10.7) in the following matrix form

$$A_\theta \cdot \phi_\theta = 0.$$

It is easy to verify that A_θ has full column rank, we deduce that $\theta_{s+1} = \dots = \theta_n = \theta'_{s+1} = \dots = \theta'_n = 0$, which contradicts to the assumption that $\theta_j \neq 0$. Thus, the only case in which there is no contradiction is $\theta_{2,j} = \theta'_{2,j}$ for all $j = 1, \dots, n$. Then we rewrite the following equations into a matrix form

$$\sum_{j=1}^n \theta_{j,1} e^{-2\pi i \theta_{j,2} k} = \sum_{j=1}^n \theta'_{j,1} e^{-2\pi i \theta_{j,2} k} \quad |k| \leq K_L. \quad (10.8)$$

We derive that

$$\tilde{A}_\theta \cdot \tilde{\phi}_\theta = 0, \quad (10.9)$$

where $\tilde{A}_\theta = (\phi_{K_L}(\theta_{1,2}), \dots, \phi_{K_L}(\theta_{1,2}))$ and $\tilde{\phi}_\theta = (\theta_{1,1} - \theta'_{1,1}, \dots, \theta_{n,1} - \theta'_{n,1})^\top$. Since \tilde{A}_θ has full column rank, we have $\tilde{\phi}_\theta = 0$, which implies $\theta_{1,j} = \theta'_{1,j}$ for all $j = 1, \dots, n$. Therefore, $\mathcal{P}_L|_U$ is injective.

Step 2. Injectivity of $D\mathcal{P}_L|_U$:

We calculate that

$$\frac{\partial \psi}{\partial \theta_{j,1}}(k) = e^{-2\pi i \theta_{j,2} k}, \quad (10.10)$$

$$\frac{\partial \psi}{\partial \theta_{j,2}}(k) = -2\pi i \cdot \theta_{j,1} k e^{-2\pi i \theta_{j,2} k}, \quad (10.11)$$

and

$$D\mathcal{P}_L(\theta) = \begin{pmatrix} \frac{\partial\psi}{\partial\theta_{1,1}}(-K_L) & \cdots & \frac{\partial\psi}{\partial\theta_{n,1}}(-K_L) & \frac{\partial\psi}{\partial\theta_{1,2}}(-K_L) & \cdots & \frac{\partial\psi}{\partial\theta_{n,2}}(-K_L) \\ \vdots & & \vdots & \vdots & & \vdots \\ \frac{\partial\psi}{\partial\theta_{1,1}}(K_L) & \cdots & \frac{\partial\psi}{\partial\theta_{n,1}}(K_L) & \frac{\partial\psi}{\partial\theta_{1,2}}(K_L) & \cdots & \frac{\partial\psi}{\partial\theta_{n,2}}(K_L) \end{pmatrix}. \quad (10.12)$$

For any $\theta \in U$, the confluent Vandermonde matrix $D\mathcal{P}_L$ has full column rank and thus $D\mathcal{P}_L|_U$ is injective.

Step 3. Estimation of $\|D\mathcal{P}_H(\theta)\|_{op}$:

Straightforward calculation gives that

$$D\mathcal{P}_H(\theta) = \begin{pmatrix} \frac{\partial\psi}{\partial\theta_{1,1}}(-K_H) & \cdots & \frac{\partial\psi}{\partial\theta_{n,1}}(-K_H) & \frac{\partial\psi}{\partial\theta_{1,2}}(-K_H) & \cdots & \frac{\partial\psi}{\partial\theta_{n,2}}(-K_H) \\ \vdots & & \vdots & \vdots & & \vdots \\ \frac{\partial\psi}{\partial\theta_{1,1}}(K_H) & \cdots & \frac{\partial\psi}{\partial\theta_{n,1}}(K_H) & \frac{\partial\psi}{\partial\theta_{1,2}}(K_H) & \cdots & \frac{\partial\psi}{\partial\theta_{n,2}}(K_H) \end{pmatrix}. \quad (10.13)$$

For any given $\theta \in U$, we have

$$\begin{aligned} \|D\mathcal{P}_H(\theta)\|_{op}^2 &\leq \|D\mathcal{P}_H(\theta)\|_F^2 = (2K_H + 1)n + \frac{4\pi^2}{3} \sum_{j=1}^n \theta_{j,1}^2 \cdot (K_H(K_H + 1)(2K_H + 1)) \\ &\leq (2K_H + 1)n + \frac{4n\pi^2 A_I^2}{3} \cdot (K_H(K_H + 1)(2K_H + 1)). \end{aligned} \quad (10.14)$$

10.4 Proof of Theorem 5.1

We notice that U is compact and convex. According to Theorem 3.1,, we only need to verify $\mathcal{P}_L|_U$ is injective and $D\mathcal{P}_L|_U(\theta)$ is injective for all $\theta \in U$.

Step 1. Injectivity of $\mathcal{P}_L|_U$:

For $\theta, \theta' \in U$, we assume that $\mathcal{P}_L(\theta) = \mathcal{P}_L(\theta')$, i.e.

$$\sum_{r=0}^R \sum_{j=1}^{n_r} \theta_{r,j,1} \cdot (-2\pi ik)^r e^{-2\pi i\theta_{r,j,2}k} = \sum_{r=0}^R \sum_{j=1}^{n_r} \theta'_{r,j,1} \cdot (-2\pi ik)^r e^{-2\pi i\theta'_{r,j,2}k}, \quad |k| \leq K_L. \quad (10.15)$$

By the similar method of the proof of Theorem 4.1, we only need to show that sources with different orders generate independent signals and the same order source with different positions generate independent signals. It then suffices to show that for $\theta_{j,2} \neq \theta'_{j,2}$, the matrix

$$\begin{pmatrix} e^{2\pi i\theta_{r,j,2}K_L} & \cdots & (2\pi iK_L)^{R_1} e^{2\pi i\theta_{r,j,2}K_L} & e^{2\pi i\theta'_{j,r,2}K_L} & \cdots & (2\pi iK_L)^{R_1} e^{2\pi i\theta'_{j,r,2}K_L} \\ \vdots & & \vdots & \vdots & & \vdots \\ e^{-2\pi i\theta_{r,j,2}K_L} & \cdots & (-2\pi iK_L)^{R_2} e^{-2\pi i\theta_{r,j,2}K_L} & e^{-2\pi i\theta'_{j,r,2}K_L} & \cdots & (-2\pi iK_L)^{R_2} e^{-2\pi i\theta'_{j,r,2}K_L} \end{pmatrix}$$

has full column rank for any R_1 and R_2 , and it is straightforward by its confluent Vandermonde matrix structure. Therefore, $\mathcal{P}_L|_U$ is injective.

Step 2. Injectivity of $D\mathcal{P}_L|_U$:

We calculate that

$$\frac{\partial\psi}{\partial\theta_{r,j,1}}(k) = (-2\pi ik)^r \cdot e^{-2\pi i\theta_{r,j,2}k}, \quad (10.16)$$

$$\frac{\partial\psi}{\partial\theta_{r,j,2}}(k) = \theta_{r,j,1} \cdot (-2\pi ik)^{r+1} \cdot e^{-2\pi i\theta_{r,j,2}k}, \quad (10.17)$$

and

$$D\mathcal{P}_L(\theta) = \begin{pmatrix} \frac{\partial\psi}{\partial\theta_{0,1,1}}(-K_L) & \cdots & \frac{\partial\psi}{\partial\theta_{R,n_R,1}}(-K_L) & \frac{\partial\psi}{\partial\theta_{1,0,2}}(-K_L) & \cdots & \frac{\partial\psi}{\partial\theta_{R,n_R,2}}(-K_L) \\ \vdots & & \vdots & \vdots & & \vdots \\ \frac{\partial\psi}{\partial\theta_{0,1,1}}(-K_L) & \cdots & \frac{\partial\psi}{\partial\theta_{R,n_R,1}}(-K_L) & \frac{\partial\psi}{\partial\theta_{0,1,2}}(-K_L) & \cdots & \frac{\partial\psi}{\partial\theta_{R,n_R,2}}(-K_L) \end{pmatrix}.$$

The confluent Vandermonde matrix structure of $D\mathcal{P}_L$ implies its injectivity for all $\theta \in U$.

Step 3. Estimation of $\|D\mathcal{P}_H(\theta)\|_{op}$:

It is clear that

$$D\mathcal{P}_H(\theta) = \begin{pmatrix} \frac{\partial\psi}{\partial\theta_{0,1,1}}(-K_H) & \cdots & \frac{\partial\psi}{\partial\theta_{R,n_R,1}}(-K_H) & \frac{\partial\psi}{\partial\theta_{0,1,2}}(-K_H) & \cdots & \frac{\partial\psi}{\partial\theta_{R,n_R,2}}(-K_H) \\ \vdots & & \vdots & \vdots & & \vdots \\ \frac{\partial\psi}{\partial\theta_{0,1,1}}(-K_H) & \cdots & \frac{\partial\psi}{\partial\theta_{R,n_R,1}}(-K_H) & \frac{\partial\psi}{\partial\theta_{0,1,2}}(-K_H) & \cdots & \frac{\partial\psi}{\partial\theta_{R,n_R,2}}(-K_H) \end{pmatrix}.$$

For any given $\theta \in U$, we have

$$\|D\mathcal{P}_H\|_{op}^2 \leq \|D\mathcal{P}_H\|_F^2 \leq \sum_{k=-K_L}^{K_L} \sum_{r=0}^R n_r (2\pi k)^{2r} (1 + 4\pi^2 k^2 A_J^2).$$

10.5 Proof of Theorem 6.1

We notice that U is compact and convex. According to Theorem 3.1, we only need to verify $\mathcal{P}_L|_U$ is injective and $D\mathcal{P}_L(\theta)$ is injective for all $\theta \in U$.

Step 1. Injectivity of $\mathcal{P}_L|_U$:

For $\theta, \theta' \in U$, we assume that $\mathcal{P}_L(\theta) = \mathcal{P}_L(\theta')$, i.e.

$$\sum_{j=1}^n \theta_{j,1} \theta_{j,2} \cdot e^{-2\pi i \theta_{j,3} \omega_k} \cdot e^{-2\pi^2 \theta_{j,2}^2 \omega_k^2} = \sum_{j=1}^n \theta'_{j,1} \theta'_{j,2} \cdot e^{-2\pi i \theta'_{j,3} \omega_k} \cdot e^{-2\pi^2 \theta'_{j,2}{}^2 \omega_k^2}. \quad (10.18)$$

Denote

$$\psi_{K_L}(\theta_{j,2}, \theta_{j,3}) = \begin{pmatrix} \theta_{j,2} \cdot e^{-2\pi i \theta_{j,3} \omega_{-K_L}} \cdot e^{-2\pi^2 \theta_{j,2}^2 \omega_{-K_L}^2} \\ \theta_{j,2} \cdot e^{-2\pi i \theta_{j,3} \omega_{-K_L+1}} \cdot e^{-2\pi^2 \theta_{j,2}^2 \omega_{-K_L+1}^2} \\ \vdots \\ \theta_{j,2} \cdot e^{-2\pi i \theta_{j,3} \omega_{K_L}} \cdot e^{-2\pi^2 \theta_{j,2}^2 \omega_{K_L}^2} \end{pmatrix}.$$

By the similar method of the proof of Theorem 4.1, we only need to show that for $(\theta_{j,2}, \theta_{j,3}) \neq (\theta'_{j,2}, \theta'_{j,3})$, $\psi_{K_L}(\theta_{j,2}, \theta_{j,3})$ and $\psi_{K_L}(\theta'_{j,2}, \theta'_{j,3})$ are linearly independent.

If $\psi_{K_L}(\theta_{j,2}, \theta_{j,3}) = a\psi_{K_L}(\theta'_{j,2}, \theta'_{j,3})$ for some $a \neq 0$, then straightforward calculation gives

$$(\omega_{-K_L}^2 - \omega_{-K_L+1}^2) (\theta_{j,2}^2 - \theta'_{j,2}{}^2) = 0.$$

By the fact that $\theta_{j,2}, \theta'_{j,2} > 0$, we have $\theta_{j,2} = \theta'_{j,2}$.

For $\theta_{j,3} \neq \theta'_{j,3}$, we have

$$(\psi_{K_L}(\theta_{j,2}, \theta_{j,3}), \psi_{K_L}(\theta_{j,2}, \theta'_{j,3})) = \theta_{j,2} \begin{pmatrix} e^{-2\pi^2 \theta_{j,2}^2 \omega_{-K_L}^2} & & \\ & \ddots & \\ & & e^{-2\pi^2 \theta_{j,2}^2 \omega_{K_L}^2} \end{pmatrix} \begin{pmatrix} e^{-2\pi i \theta_{j,3} \omega_{-K_L}} & e^{-2\pi i \theta'_{j,3} \omega_{-K_L}} \\ e^{-2\pi i \theta_{j,3} \omega_{-K_L+1}} & e^{-2\pi i \theta'_{j,3} \omega_{-K_L+1}} \\ \vdots & \vdots \\ e^{-2\pi i \theta_{j,3} \omega_{K_L}} & e^{-2\pi i \theta'_{j,3} \omega_{K_L}} \end{pmatrix}.$$

Clearly, $(\psi_{K_L}(\theta_{j,2}, \theta_{j,3}), \psi_{K_L}(\theta_{j,2}, \theta'_{j,3}))$ has full column rank, and $\psi_{K_L}(\theta_{j,2}, \theta_{j,3})$ and $\psi_{K_L}(\theta_{j,2}, \theta'_{j,3})$ are thus linearly independent.

Therefore, we conclude that $\mathcal{P}_L|_U$ is injective.

Step 2. Injectivity of $D\mathcal{P}_L|_U$:

We calculate that

$$\frac{\partial \psi}{\partial \theta_{j,1}}(\omega_k) = \theta_{j,2} \cdot e^{-2\pi i \theta_{j,3} \omega_k} \cdot e^{-2\pi^2 \theta_{j,2}^2 \omega_k^2}, \quad (10.19)$$

$$\frac{\partial \psi}{\partial \theta_{j,2}}(\omega_k) = (\theta_{j,1} - 4\pi^2 \theta_{j,1} \theta_{j,2}^2 \omega_k^2) \cdot e^{-2\pi i \theta_{j,3} \omega_k} \cdot e^{-2\pi^2 \theta_{j,2}^2 \omega_k^2} \quad (10.20)$$

$$\frac{\partial \psi}{\partial \theta_{j,3}}(\omega_k) = -2\pi i \omega_k \theta_{j,1} \theta_{j,2} \cdot e^{-2\pi i \theta_{j,3} \omega_k} \cdot e^{-2\pi^2 \theta_{j,2}^2 \omega_k^2}, \quad (10.21)$$

and

$$D\mathcal{P}_L = \begin{pmatrix} \frac{\partial \psi}{\partial \theta_{1,1}}(\omega_{-K_L}) & \cdots & \frac{\partial \psi}{\partial \theta_{n,1}}(\omega_{-K_L}) & \frac{\partial \psi}{\partial \theta_{1,2}}(\omega_{-K_L}) & \cdots & \frac{\partial \psi}{\partial \theta_{n,2}}(\omega_{-K_L}) & \frac{\partial \psi}{\partial \theta_{1,3}}(\omega_{-K_L}) & \cdots & \frac{\partial \psi}{\partial \theta_{n,3}}(\omega_{-K_L}) \\ \vdots & & \vdots & \vdots & & \vdots & \vdots & & \vdots \\ \frac{\partial \psi}{\partial \theta_{1,1}}(\omega_{K_L}) & \cdots & \frac{\partial \psi}{\partial \theta_{n,1}}(\omega_{K_L}) & \frac{\partial \psi}{\partial \theta_{1,2}}(\omega_{K_L}) & \cdots & \frac{\partial \psi}{\partial \theta_{n,2}}(\omega_{K_L}) & \frac{\partial \psi}{\partial \theta_{1,3}}(\omega_{K_L}) & \cdots & \frac{\partial \psi}{\partial \theta_{n,3}}(\omega_{K_L}) \end{pmatrix}.$$

Let $\alpha_{j,t} = \left(\frac{\partial \psi}{\partial \theta_{j,t}}(\omega_{-K_L}), \dots, \frac{\partial \psi}{\partial \theta_{j,t}}(\omega_{K_L}) \right)^\top$, for $j = 1, \dots, n$ and $t = 1, 2, 3$. We write

$$\begin{aligned}\xi_{j,1} &= \left(e^{-2\pi i \theta_{j,3} \omega_{-K_L}} \cdot e^{-2\pi^2 \theta_{j,2}^2 \omega_{-K_L}^2}, \dots, e^{-2\pi i \theta_{j,3} \omega_{K_L}} \cdot e^{-2\pi^2 \theta_{j,2}^2 \omega_{K_L}^2} \right)^\top, \\ \xi_{j,2} &= \left(\omega_{-K_L} e^{-2\pi i \theta_{j,3} \omega_{-K_L}} \cdot e^{-2\pi^2 \theta_{j,2}^2 \omega_{-K_L}^2}, \dots, \omega_{K_L} e^{-2\pi i \theta_{j,3} \omega_{K_L}} \cdot e^{-2\pi^2 \theta_{j,2}^2 \omega_{K_L}^2} \right)^\top, \\ \xi_{j,3} &= \left(\omega_{-K_L}^2 e^{-2\pi i \theta_{j,3} \omega_{-K_L}} \cdot e^{-2\pi^2 \theta_{j,2}^2 \omega_{-K_L}^2}, \dots, \omega_{K_L}^2 e^{-2\pi i \theta_{j,3} \omega_{K_L}} \cdot e^{-2\pi^2 \theta_{j,2}^2 \omega_{K_L}^2} \right)^\top.\end{aligned}$$

Then, we have $\alpha_{j,1} = \theta_{j,2} \xi_{j,1}$, $\alpha_{j,2} = \theta_{j,1} \xi_{j,1} - 4\pi^2 \theta_{j,1} \theta_{j,2}^2 \xi_{j,3}$, $\alpha_{j,3} = -2\pi i \theta_{j,1} \theta_{j,2} \xi_{j,2}$.

Clearly, $\xi_{j,1}$, $\xi_{j,2}$, and $\xi_{j,3}$ are linearly independent. Then, for $(\theta_{j,2}, \theta_{j,3}) \neq (\theta'_{j,2}, \theta'_{j,3})$, it is easy to see that (1) $\xi_{j,1}$ and $\xi_{j',2}$ are linearly independent, (2) $\xi_{j,1}$ and $\xi_{j',3}$ are linearly independent. By the similar argument in Step 1, we can verify that (3) $\xi_{j,t}$ and $\xi_{j',t}$ are linearly independent for $t = 1, 2, 3$.

If $\xi_{j,2} = a \xi_{j',3}$ for some $a \neq 0$, we first consider the first two elements of both vectors, straightforward calculation gives

$$e^{-2\pi^2(\omega_{-K_L}^2 - \omega_{-K_L+1}^2)}(\theta_{j,2}^2 - \theta_{j',2}^2) = \left| \frac{\omega_{-K_L}}{\omega_{-K_L+1}} \right| \Rightarrow e^{-2\pi^2(2K_L-1)(\theta_{j,2}^2 - \theta_{j',2}^2)} = \frac{K_L}{K_L - 1}. \quad (10.22)$$

Clearly, the identity holds only if $\theta_{j,2} \neq \theta_{j',2}$. However, one can recursively derive the similar identities:

$$e^{-2\pi^2(2K_L-3)(\theta_{j,2}^2 - \theta_{j',2}^2)} = \frac{K_L - 1}{K_L - 2}, \quad e^{-2\pi^2(2K_L-5)(\theta_{j,2}^2 - \theta_{j',2}^2)} = \frac{K_L - 2}{K_L - 3}. \quad (10.23)$$

Taking the quotient for the above identities on both sides, we have

$$e^{4\pi^2(\theta_{j,2}^2 - \theta_{j',2}^2)} = \frac{K_L}{K_L - 2}, \quad e^{4\pi^2(\theta_{j,2}^2 - \theta_{j',2}^2)} = \frac{K_L - 1}{K_L - 3}, \quad (10.24)$$

which is impossible. Therefore, $\xi_{j,2}$ and $\xi_{j,3}$ are linearly independent.

We showed that $\{\xi_{j,1}, \xi_{j,2}, \xi_{j,3}, \xi_{j',1}, \xi_{j',2}, \xi_{j',3}\}$ are linearly independent, which leads to the linear independence of $\{\alpha_{j,1}, \alpha_{j,2}, \alpha_{j,3}, \alpha_{j',1}, \alpha_{j',2}, \alpha_{j',3}\}$.

Thus, for all $\theta \in U$, $D\mathcal{P}_L$ has full column rank and is injective.

Step 3. Estimation of $\|D\mathcal{P}_H(\theta)\|_{op}$:

It is clear that

$$D\mathcal{P}_H = \begin{pmatrix} \frac{\partial \psi}{\partial \theta_{1,1}}(\omega_{-K_H}) & \cdots & \frac{\partial \psi}{\partial \theta_{n,1}}(\omega_{-K_H}) & \frac{\partial \psi}{\partial \theta_{1,2}}(\omega_{-K_H}) & \cdots & \frac{\partial \psi}{\partial \theta_{n,2}}(\omega_{-K_H}) & \frac{\partial \psi}{\partial \theta_{1,3}}(\omega_{-K_H}) & \cdots & \frac{\partial \psi}{\partial \theta_{n,3}}(\omega_{-K_H}) \\ \vdots & & \vdots & \vdots & & \vdots & \vdots & & \vdots \\ \frac{\partial \psi}{\partial \theta_{1,1}}(\omega_{K_H}) & \cdots & \frac{\partial \psi}{\partial \theta_{n,1}}(\omega_{K_H}) & \frac{\partial \psi}{\partial \theta_{1,2}}(\omega_{K_H}) & \cdots & \frac{\partial \psi}{\partial \theta_{n,2}}(\omega_{K_H}) & \frac{\partial \psi}{\partial \theta_{1,3}}(\omega_{K_H}) & \cdots & \frac{\partial \psi}{\partial \theta_{n,3}}(\omega_{K_H}) \end{pmatrix}.$$

For any given $\theta \in U$, we have

$$\|D\mathcal{P}_H\|_{op}^2 \leq \|D\mathcal{P}_H\|_F^2 \leq \sum_{j=1}^n \sum_{k=-K_H}^{K_H} (\theta_{j,1}^2 + \theta_{j,2}^2 + 16\pi^4 \theta_{j,1}^2 \theta_{j,2}^4 k^4 + 4\pi^2 \theta_{j,1}^2 \theta_{j,2}^2 k^2) \cdot e^{-4\pi^2 \theta_{j,2}^2 k^2} \leq C_3,$$

where C_3 is independent on K_H , due to the convergence of the series $\sum_k k^{s_1} e^{-s_2 k^2}$ for all $s_1 \in \mathbb{N}$ and $s_2 > 0$.

References

- [1] V. Khaidukov, E. Landa, and T. J. Moser, “Diffraction imaging by focusing-defocusing: An outlook on seismic superresolution,” *Geophysics*, vol. 69, no. 6, pp. 1478–1490, 2004.
- [2] H. Greenspan, “Super-resolution in medical imaging,” *The computer journal*, vol. 52, no. 1, pp. 43–63, 2009.
- [3] J. Odendaal, E. Barnard, and C. Pistorius, “Two-dimensional superresolution radar imaging using the music algorithm,” *IEEE Transactions on Antennas and Propagation*, vol. 42, no. 10, pp. 1386–1391, 1994.
- [4] M. J. Rust, M. Bates, and X. Zhuang, “Sub-diffraction-limit imaging by stochastic optical reconstruction microscopy (storm),” *Nature methods*, vol. 3, no. 10, p. 793, 2006.
- [5] S. Vessella, “A continuous dependence result in the analytic continuation problem,” *Forum Mathematicum*, vol. 11, 1999.
- [6] L. Demanet and A. Townsend, “Stable extrapolation of analytic functions,” *Foundations of Computational Mathematics*, vol. 19, pp. 297–331, 2019.
- [7] M. Isaev and R. G. Novikov, “Hölder-logarithmic stability in fourier synthesis,” *arXiv preprint arXiv:2005.01414*, 2020.
- [8] R. Prony, “Essai expérimental et analytique,” *J. de l’Ecole Polytechnique (Paris)*, vol. 1, no. 2, pp. 24–76, 1795.
- [9] R. Schmidt, “Multiple emitter location and signal parameter estimation,” *IEEE Transactions on Antennas and Propagation*, vol. 34, no. 3, pp. 276–280, 1986.
- [10] R. Roy and T. Kailath, “Esprit-estimation of signal parameters via rotational invariance techniques,” *IEEE Transactions on Acoustics, Speech, and Signal Processing*, vol. 37, no. 7, pp. 984–995, 1989.
- [11] Y. Hua and T. K. Sarkar, “Matrix pencil method for estimating parameters of exponentially damped/undamped sinusoids in noise,” *IEEE Transactions on Acoustics, Speech, and Signal Processing*, vol. 38, no. 5, pp. 814–824, 1990.
- [12] W. Li, W. Liao, and A. Fannjiang, “Super-resolution limit of the esprit algorithm,” *IEEE transactions on information theory*, vol. 66, no. 7, pp. 4593–4608, 2020.
- [13] W. Liao and A. C. Fannjiang, “Music for single-snapshot spectral estimation: Stability and super-resolution,” *Applied and Computational Harmonic Analysis*, vol. 40, no. 1, pp. 33–67, 2016.
- [14] A. Moitra, “Super-resolution, extremal functions and the condition number of vandermonde matrices,” in *Proceedings of the Forty-seventh Annual ACM Symposium on Theory of Computing*, STOC ’15, (New York, NY, USA), pp. 821–830, ACM, 2015.

- [15] R. Tibshirani, “Regression shrinkage and selection via the lasso,” *Journal of the Royal Statistical Society. Series B (Methodological)*, vol. 58, no. 1, pp. 267–288, 1996.
- [16] E. J. Candès and C. Fernandez-Granda, “Towards a mathematical theory of super-resolution,” *Communications on Pure and Applied Mathematics*, vol. 67, no. 6, pp. 906–956, 2014.
- [17] E. J. Candès and C. Fernandez-Granda, “Super-resolution from noisy data,” *Journal of Fourier Analysis and Applications*, vol. 19, no. 6, pp. 1229–1254, 2013.
- [18] G. Tang, B. N. Bhaskar, and B. Recht, “Near minimax line spectral estimation,” *IEEE Transactions on Information Theory*, vol. 61, no. 1, pp. 499–512, 2014.
- [19] Y. Chi and M. F. Da Costa, “Harnessing sparsity over the continuum: Atomic norm minimization for superresolution,” *IEEE Signal Processing Magazine*, vol. 37, no. 2, pp. 39–57, 2020.
- [20] Y. De Castro and F. Gamboa, “Exact reconstruction using beurling minimal extrapolation,” *Journal of Mathematical Analysis and applications*, vol. 395, no. 1, pp. 336–354, 2012.
- [21] Z. Yang, J. Li, P. Stoica, and L. Xie, “Chapter 11 - sparse methods for direction-of-arrival estimation,” in *Academic Press Library in Signal Processing, Volume 7* (R. Chelappa and S. Theodoridis, eds.), pp. 509–581, Academic Press, 2018.
- [22] C. Poon and G. Peyré, “Multidimensional sparse super-resolution,” *SIAM Journal on Mathematical Analysis*, vol. 51, no. 1, pp. 1–44, 2019.
- [23] D. L. Donoho, “Superresolution via sparsity constraints,” *SIAM journal on mathematical analysis*, vol. 23, no. 5, pp. 1309–1331, 1992.
- [24] L. Demanet and N. Nguyen, “The recoverability limit for superresolution via sparsity,” *arXiv preprint arXiv:1502.01385*, 2015.
- [25] D. Batenkov, G. Goldman, and Y. Yomdin, “Super-resolution of near-colliding point sources,” *Information and Inference: A Journal of the IMA*, 05 2020. iaaa005.
- [26] D. Batenkov, L. Demanet, G. Goldman, and Y. Yomdin, “Conditioning of partial nonuniform fourier matrices with clustered nodes,” *SIAM Journal on Matrix Analysis and Applications*, vol. 41, no. 1, pp. 199–220, 2020.
- [27] W. Li and W. Liao, “Stable super-resolution limit and smallest singular value of restricted fourier matrices,” *Applied and Computational Harmonic Analysis*, vol. 51, pp. 118–156, 2021.
- [28] P. Liu and H. Zhang, “A theory of computational resolution limit for line spectral estimation,” *IEEE Transactions on Information Theory*, vol. 67, no. 7, pp. 4812–4827, 2021.

- [29] P. Liu and H. Zhang, “A mathematical theory of the computational resolution limit in one dimension,” *Applied and Computational Harmonic Analysis*, vol. 56, pp. 402–446, 2022.
- [30] P. Liu and H. Zhang, “A mathematical theory of computational resolution limit in multi-dimensional spaces*,” *Inverse Problems*, vol. 37, p. 104001, sep 2021.
- [31] P. Liu and H. Ammari, “Super-resolution of positive near-colliding point sources,” *Information and Inference: A Journal of the IMA*, vol. 12, no. 4, pp. 3087–3111, 2023.
- [32] P. Liu, S. Yu, O. Sabet, L. Pelkmans, and H. Ammari, “Mathematical foundation of sparsity-based multi-snapshot spectral estimation,” *Applied and Computational Harmonic Analysis*, vol. 73, p. 101673, 2024.
- [33] D. Batenkov and N. Diab, “Super-resolution of generalized spikes and spectra of confluent vandermonde matrices,” *Applied and Computational Harmonic Analysis*, vol. 65, pp. 181–208, 2023.
- [34] D. Glasner, S. Bagon, and M. Irani, “Super-resolution from a single image,” in *2009 IEEE 12th International Conference on Computer Vision*, pp. 349–356, 2009.
- [35] W. T. Freeman, T. R. Jones, and E. C. Pasztor, “Example-based super-resolution,” *IEEE Computer graphics and Applications*, vol. 22, no. 2, pp. 56–65, 2002.
- [36] H. Chang, D.-Y. Yeung, and Y. Xiong, “Super-resolution through neighbor embedding,” in *Proceedings of the 2004 IEEE Computer Society Conference on Computer Vision and Pattern Recognition, 2004. CVPR 2004.*, vol. 1, pp. I–I, 2004.
- [37] R. Timofte, V. De, and L. V. Gool, “Anchored neighborhood regression for fast example-based super-resolution,” in *2013 IEEE International Conference on Computer Vision*, pp. 1920–1927, 2013.
- [38] J. Yang, J. Wright, T. Huang, and Y. Ma, “Image super-resolution as sparse representation of raw image patches,” in *2008 IEEE Conference on Computer Vision and Pattern Recognition*, pp. 1–8, 2008.
- [39] J. Yang, Z. Wang, Z. Lin, S. Cohen, and T. Huang, “Coupled dictionary training for image super-resolution,” *IEEE transactions on image processing*, vol. 21, no. 8, pp. 3467–3478, 2012.
- [40] C. Dong, C. C. Loy, K. He, and X. Tang, “Image super-resolution using deep convolutional networks,” *IEEE Transactions on Pattern Analysis and Machine Intelligence*, vol. 38, no. 2, pp. 295–307, 2016.
- [41] V. Nair and G. E. Hinton, “Rectified linear units improve restricted boltzmann machines,” in *Proceedings of the 27th international conference on machine learning (ICML-10)*, pp. 807–814, 2010.

- [42] W. Ouyang, X. Wang, X. Zeng, S. Qiu, P. Luo, Y. Tian, H. Li, S. Yang, Z. Wang, C.-C. Loy, *et al.*, “Deepid-net: Deformable deep convolutional neural networks for object detection,” in *Proceedings of the IEEE conference on computer vision and pattern recognition*, pp. 2403–2412, 2015.
- [43] W. Ouyang and X. Wang, “Joint deep learning for pedestrian detection,” in *Proceedings of the IEEE international conference on computer vision*, pp. 2056–2063, 2013.
- [44] Y. Zhang, L. Sun, C. Yan, X. Ji, and Q. Dai, “Adaptive residual networks for high-quality image restoration,” *IEEE Transactions on Image Processing*, vol. 27, no. 7, pp. 3150–3163, 2018.
- [45] R. Dahl, M. Norouzi, and J. Shlens, “Pixel recursive super resolution,” in *Proceedings of the IEEE international conference on computer vision*, pp. 5439–5448, 2017.
- [46] Y. Jo, S. Wug Oh, P. Vajda, and S. Joo Kim, “Tackling the ill-posedness of super-resolution through adaptive target generation,” in *2021 IEEE/CVF Conference on Computer Vision and Pattern Recognition (CVPR)*, pp. 16231–16240, 2021.
- [47] C. Ledig, L. Theis, F. Huszár, J. Caballero, A. Cunningham, A. Acosta, A. Aitken, A. Tejani, J. Totz, Z. Wang, *et al.*, “Photo-realistic single image super-resolution using a generative adversarial network,” in *Proceedings of the IEEE conference on computer vision and pattern recognition*, pp. 4681–4690, 2017.
- [48] Z. Wang, D. Liu, J. Yang, W. Han, and T. Huang, “Deep networks for image super-resolution with sparse prior,” in *Proceedings of the IEEE international conference on computer vision*, pp. 370–378, 2015.
- [49] X. Gao and H. Xiong, “A hybrid wavelet convolution network with sparse-coding for image super-resolution,” in *2016 IEEE International Conference on Image Processing (ICIP)*, pp. 1439–1443, 2016.
- [50] Z. Wang, J. Chen, and S. C. Hoi, “Deep learning for image super-resolution: A survey,” *IEEE transactions on pattern analysis and machine intelligence*, vol. 43, no. 10, pp. 3365–3387, 2020.
- [51] W. Yang, X. Zhang, Y. Tian, W. Wang, J.-H. Xue, and Q. Liao, “Deep learning for single image super-resolution: A brief review,” *IEEE Transactions on Multimedia*, vol. 21, no. 12, pp. 3106–3121, 2019.
- [52] J. P. Cunningham and Z. Ghahramani, “Linear dimensionality reduction: Survey, insights, and generalizations,” *The Journal of Machine Learning Research*, vol. 16, no. 1, pp. 2859–2900, 2015.
- [53] L. Li, M. Hurtado, F. Xu, B. C. Zhang, T. Jin, T. J. Xui, M. N. Stevanovic, and A. Nehorai, “A survey on the low-dimensional-model-based electromagnetic imaging,” *Foundations and Trends® in Signal Processing*, vol. 12, no. 2, pp. 107–199, 2018.

- [54] S. Osher, Z. Shi, and W. Zhu, “Low dimensional manifold model for image processing,” *SIAM Journal on Imaging Sciences*, vol. 10, no. 4, pp. 1669–1690, 2017.
- [55] K. Berahmand, F. Daneshfar, E. S. Salehi, Y. Li, and Y. Xu, “Autoencoders and their applications in machine learning: a survey,” *Artificial Intelligence Review*, vol. 57, no. 2, p. 28, 2024.
- [56] G. S. Alberti, Á. Arroyo, and M. Santacesaria, “Inverse problems on low-dimensional manifolds,” *Nonlinearity*, vol. 36, no. 1, p. 734, 2022.
- [57] H. Mohammad, M. Y. Waziri, and S. A. Santos, “A brief survey of methods for solving nonlinear least-squares problems,” *Numerical Algebra, Control & Optimization*, vol. 9, no. 1, pp. 1–13, 2019.
- [58] M. Vetterli, P. Marziliano, and T. Blu, “Sampling signals with finite rate of innovation,” *IEEE Transactions on Signal Processing*, vol. 50, no. 6, pp. 1417–1428, 2002.
- [59] G. Ongie and M. Jacob, “Off-the-grid recovery of piecewise constant images from few fourier samples,” *SIAM Journal on Imaging Sciences*, vol. 9, no. 3, pp. 1004–1041, 2016.